Title: Nutritional Immunity and Antibiotic Drug Treatments Influence Microbial Composition but Fail to Eliminate Urethral Catheter Biofilms in Recurrently Catheterized Patients

Running Title: Urethral Catheter Biofilm Dynamics in Spinal Cord-Injured Patients

Authors: Yanbao Yu[a^], Harinder Singh[a^], Tamara Tsitrin[a], Keehwan Kwon[a*], Shiferaw Bekele[a**], Rodrigo V. Eguez[a], Yi-Han Lin[a], Patricia Sikorski[a***], Kelvin J. Moncera[b****], Manolito G. Torralba[b], Lisa Morrow[c], Randall Wolcott[c], Karen E. Nelson[ab] and Rembert Pieper[a#]

[a] J. Craig Venter Institute, 9605 Medical Center Drive, Rockville, Maryland 20850;

[b] J. Craig Venter Institute, 4120 Capricorn Lane, La Jolla, California 92037;

[c] Southwest Regional Wound Care Center, 2002 Oxford Avenue, Lubbock, Texas 79410;

* GlaxoSmithKline, 1250 S. Collegeville Rd., Collegeville, PA 19426;

** University of Maryland Medical Center, 655 W Baltimore Street, Baltimore, MD 21201;

*** Laboratory of Parasitic Diseases, NIAID, NIH, 4 Memorial Drive, Bethesda, MD 20892 and Department of Microbiology and Immunology, Georgetown University, 3900 Reservoir Road, N.W., Washington, DC 20057;

**** Western University of Health Sciences, College of Osteopathic Medicine of the Pacific, 309 E 2nd St, Pomona, CA 91766;

[^] Authors contributed equally

[#]Corresponding author: Rembert Pieper, Email: rembertpieper2@gmail.com; Tel: (301) 795-7605

Abstract

Polymicrobial biofilms that form on indwelling urethral catheters used by neurogenic bladder patients are known to recur following catheter replacements. Uropathogens dominate in catheter biofilms (CBs), grow and disperse as multi-cellular aggregates. Their microbial complexity, the characteristics of host immune responses and the molecular crosstalk in this ecosystem are incompletely understood. By surveying eight patients over up to six months with meta-omics analysis methods, we shed new light on the longitudinal microbial dynamics in CBs and the microbial-host crosstalk. There was evidence of chronic innate immune responses in all patients. Pathogens dominated the microbial contents. *Proteus mirabilis* often out-competed other species in cases of salt encrustation of catheters. The examination of proteomes in CBs and associated urinary pellets revealed many abundant bacterial systems for transition metal ion (TMI) acquisition. TMIs are sequestered by effector proteins released by activated neutrophils and urothelial cells, such as lactotransferrin and calgranulins, which were abundant in the host proteomes. We identified positive quantitative correlations among systems responsible for siderophore biosynthesis, TMI/siderophore uptake and TMI cellular import in bacterial species, suggesting competition for TMIs to support their metabolism and growth in CBs. *Enterococcus faecalis* was prevalent as a cohabitant of CBs and expressed three lipoproteins with apparent TMI acquisition functions. Fastidious anaerobic bacteria such as *Veillonella*, *Actinobaculum*, and *Bifidobacterium* grew in CB communities that appeared to be oxygen starved. Finally, antibiotic drug treatments were shown to influence microbial composition of CBs but failed to prevent re-colonization of urethral catheters with persisting and/or drug-resistant newly emerging pathogens.

Introduction

Urethral catheter-associated urinary tract infection (CAUTI) is the most common type of complicated UTI. CAUTIs have a higher risk of recurrence, pyelonephritis and bacteremia than uncomplicated UTIs in nosocomial environments (1-3). Asymptomatic cases are usually diagnosed as catheter-associated asymptomatic bacteriuria (CAASB). The use of nearly 100 million urethral catheters per year worldwide, the 3% to 10% incidence of bacteriuria over 24 hours following patient catheterization and an average bladder catheter insertion time of 72 h (2) suggest an estimated 9 to 27 million CAUTI cases per year globally. Among the most common causes are *Escherichia coli*, *Klebsiella pneumoniae*, *Pseudomonas aeruginosa*, *Proteus mirabilis*, *Enterococcus* and *Candida spp.* (1, 3, 4). Indwelling Foley catheters are often used by patients with anatomical urinary tract abnormalities and neurogenic bladder syndrome and retained in the urinary tract for one week or longer. Microbial colonization is difficult to avoid even when catheters are regularly replaced, and antibiotic drug treatments are administered. Bacteria adapted to form biofilms (*e.g.*, *Enterococcus faecalis*, *P. aeruginosa*, and *E. coli*) and those that degrade urea and use ammonia as a nitrogen source (*e.g.*, *Proteus* and *Providencia spp.*) dominate microbial communities that form on catheter surfaces (3, 5, 6). Urea degradation alkalinizes the pH of urine and triggers the precipitation of phosphate salt crystals in this milieu, thus increasing the risk of luminal occlusion and complications such as urinary stones and kidney infections (3). Unless specific risk factors exist (*e.g.*, a compromised immune system or pregnancy), clinical guidelines do not recommend the use of antibiotics for CAASB (7). Of major concern are the genetically acquired and innate resistances of CAASB-associated bacteria against several classes of antibiotic drugs. Most of them belong to the ESKAPE group of pathogens (8). Understanding the mechanisms that drive microbial cohabitation and competition in urethral catheter biofilms (CBs) may lead to new approaches to prevent or disrupt their formation.

The pathogenesis of UTI and CAUTI has been studied extensively in the context of *E. coli* and *P. mirabilis* (4, 9-12). The innate immune system has a critical role in the recognition of and defense against invading pathogens. Their surface molecular patterns are recognized by urothelial cell effectors such as immunoglobulin A and lipopolysaccharide-binding protein. The presentation to Toll-like receptors (TLRs) triggers cytokine release and signaling events that result in leukocyte infiltration. Neutrophils are the main type of immune cells attacking and phagocytosing microbial intruders (13). Pathogen clearance results from the activities of neutrophil granular effector proteins and reactive oxygen species (ROS) as well as extracellular trapping (14, 15). Investigations of *E. coli* have implicated the neutrophil cyclooxygenase-2 in the pathogenesis of recurrent UTI (16). Recurrence is influenced by host susceptibility to and the urovirulence of strains that colonize the human intestinal tract (17).

Type I fimbriae, which are expressed by many Gram-negative bacteria, are thought to initiate mucosal colonization by binding to mannoslyated uroplakins, glycoproteins that coat the surface of urothelial umbrella cells (18). *Proteus mirabilis* produces several types of fimbriae of which the best characterized ones are the MR/P, UCF and PMF fimbriae (11). This species is the major cause of encrusted CBs where struvite and apatite minerals are deposited on catheter surfaces, triggered by urinary pH increase (3, 9, 11). Encrustation refers to the deposition of these minerals on the catheter surface along with the bacteria that thrive in this milieu. Bacterial cells in such biofilms can disperse and recolonize unoccupied catheter surfaces via swarming and adherence, processes that mediate ascendance to the kidneys and enhanced risk of pyelonephritis and urosepsis (3). The mechanisms that control microbial CB dynamics over time are complex and implicate the availability of nutrients such as carbohydrates, nitrogen, and transition metal ions (TMIs). Iron and zinc are sequestered by the innate immune system during infections (9, 19, 20). Non-encrusted biofilms have been linked to the deposition of host proteins such as fibrinogen on catheter surfaces to which bacteria adhere (3, 4). Some biofilms have a

mucoid consistency due to production of extracellular polysaccharides that encapsulate bacterial cells and impede their killing by phagocytic cells. They have also been linked to renal complications by blocking urine flow (3).

Culture-based methods have shown that CBs typically harbor more than a single microbial organism (5, 6, 21). Culture-independent metagenomic surveys have identified fastidious microbes including genera such as *Actinomyces*, *Stenotrophomonas*, *Corynebacterium*, and *Finegoldia spp*. in CBs (22, 23). While these findings indicate higher microbial diversity and the ability of strictly anaerobic bacteria to colonize catheter surfaces, to what extent fastidious microbes compete with typical uropathogens and cause inflammation in the host is unclear. A few studies have analyzed microbial profiles in urine sediments or CBs pertaining to long-term catheterization of patients. One study reported high prevalence of *E. coli*, *P. mirabilis*, and *Providencia stuartii* strains in the context of persistent bacteriuria in patients catheterized over four or more weeks (24). In a study examining 4,500 urine samples from repeatedly catheterized spinal cord-injured patients, the incidences of UTI with one and two or more identified bacterial species were 45% and 15%, respectively (25). A third study revealed polymicrobial colonization by two to four common uropathogens in 20 patients (26). Notably, antibiotic treatments altered the composition of CBs and failed to clear pathogens from the patients' urinary tracts (26).

Bladder catheterization itself was reported to cause sterile inflammation in a murine model, with CD^{45+} neutrophils as the main infiltrating immune cells. Using this model, *E. coli* and *E. faecalis* infections were shown to cause urothelial barrier disruption and further immune cell infiltration (27). Pyuria is known to occur in patients with indwelling catheters independent of the symptomology (7). Our recent work revealed neutrophil and complement system activation at similar levels in patients diagnosed with CAASB and CAUTI after catheterization at a single timepoint (28). Here, we publish the first comprehensive analyses of catheter biofilms associated with recurrent catheterization of patients. We used 16S rRNA taxonomic and proteomic analyses,

and further validated results of the host-microbial crosstalk with biochemical and microbial culture methods.

Results

Patient cohort, antibiotic treatments and phenotypic observations.

We enrolled two female and seven male human subjects of either hispanic or caucasian ethnicities. All of them had spinal cord injuries and suffered from neurogenic bladder syndrome. Comorbidities were chronically infected wounds. During the patient visits for wound treatment, indwelling bladder catheters were usually replaced. All patients received topical wound treatments with antibiotic drugs. Systemic antibiotic treatments over a limited time pertained to three patients while this study was conducted. The drug treatment regimens and other medical data are provided in Table S1 (Suppl. Data). Patient P6 was diagnosed with a renal infection a month after specimen collections ended, probably via ascension of catheter-associated pathogens to the kidneys. UTI symptoms were not reported by patients while the study was performed, which is consistent with diagnoses of CAASB. Catheters were replaced in 1- to 3-week intervals to reduce risk of CAUTI and renal complications. We analyzed urine sediments collected as centrifugal pellets from catheter collection bags and biofilms extracted from external and internal catheter surfaces. The terms used for these specimens are UP and CB, respectively, and are from here on. They were collected longitudinally from patients over 2 to 6 months, ranging from 4 to 15 timepoints. Some timepoints were represented by only a CB, a UP or both types of samples. Catheter encrustation was observed for several samples from P4, P5, P6, and P7 (Table S1, Suppl. Data). The variation in CB biomasses among the patients is displayed in Fig. 1. P6, the patient suffering a renal infection, revealed the highest average CB biomass. Four patients (P2, P4, P7, and P8) revealed only moderate variances in biomasses.

145 *Metagenomic data suggest polymicrobial colonization of catheters recurring in individual patients.*

146 Compared to microbial cultures, 16S rRNA sequencing is a less biased method to determine the
147 taxonomic composition of a microbial community. UP and CB samples derived from 8 patients
148 were subjected to 16S rRNA gene analysis. The data suggested the presence of 1 to 15 distinct
149 bacterial genera in 112 specimens (Dataset S2, Suppl. Data). Species-level resolution is not
150 achieved by sequencing the V1-V3 region of 16S rRNA. Forty genera with operational taxonomic
151 unit (OTU) abundances greater than 0.07% (arithmetic mean) were identified. Resolution at the
152 genus level only allows inferences of the presence of bacteria causing UTI and the urogenital
153 microbiome. Most prevalent were Enterobacteriaceae family members and *Enterococcus*. Less
154 prevalent were *Staphylococcus* and *Aerococcus*. Among fastidious organisms, we identified
155 genera belonging to Actinobacteria, Bacteroides and Fusobacteria. The same genera were often
156 repeatedly identified in samples from a distinct patient, suggesting the biological recurrence of the
157 bacteria in sequentially replaced catheters. There was evidence of abrupt changes in the
158 taxonomic composition for some cases that we elaborate on in a later section. Among the genera
159 rarely associated with pathogenesis in the urinary tract were *Bordetella*, *Globicatella* and
160 *Haemophilus*. As shown in Fig. 2, the bacterial genus diversity was moderately lower in salt-
161 encrusted biofilms (P4, P6, and P7) compared to non-encrusted biofilms (P1, P2, and P8). P5
162 datasets were split into these groups as salt crystals were observed only for three early collection
163 timepoints. This data supports the notion that phosphate salt deposition on catheter surfaces
164 favors growth of the urease-producing *Proteus/Providencia* group of bacteria (29). Quantitative
165 information for OTUs from 16S rRNA sequencing data is of limited value due to differences in the
166 16S rRNA gene amplification efficiencies (30). 16S rDNA taxonomic assignments were also useful
167 to customize databases for proteomic analysis.
168

Metaproteomic data reveal dominance of P. mirabilis strains in salt-encrusted CBs and the ability of fastidious bacteria to persist in longitudinally profiled CBs.

Metaproteomic database searches were performed with iterative adaptations to the composition of protein sequence databases (details in Methods section) guided by 16S rRNA results. This process allowed us to: 1. identify the correct microbial species from a given genus, most relevant in cases where more than a single species from a genus is known to colonize the human urinary tract (e.g., *Proteus, Klebsiella, Citrobacter, Enterobacter, Enterococcus, Staphylococcus, Aerococcus, Actinobaculum, Bifidobacterium,* and *Candida*); 2. select several species of the Enterobacteriaceae family for quantitative analyses only if evidence of their contributions to a sample was strong, thus avoiding incorrect peptide-spectral match assignments to orthologs with high sequence homology; 3. conduct species-specific pan-proteome database searches to assess whether key proteins were missed by analyzing data from only a single genotype (strain). The latter was most insightful for *E. coli* due to a high number of sequenced strains and the identification of plasmid-encoded virulence and antibiotic resistance proteins for all species. The Table S3 (Suppl. Data) contains the protein sequence databases used for iterative searches to selectively identify the species for quantitative proteomic analyses applied to all 121 samples, including 42 collection timepoint-matched UP and CB samples. P3 was excluded from further analysis due to a low number of samples. Quantified at the microbial species level, the data is displayed in longitudinal UP and CB sample series in the graphics of Fig. 3. We were confident that this data accounted for most of the microbial biomasses. Comparisons of equivalent timepoints (16S rRNA data vs. proteomics) suggest that low abundance microbial constituents present in samples according to 16S rRNA data were absent in proteomic profiles, consistent with the notion that lower protein detection limits for such species were reached.

193 Microbial *in vitro* culture methods were used to verify species identities and recover isolates for
194 drug susceptibility tests (DSTs). Specimens were typically stored at -80˚C prior to revival of the
195 microbial strains on media under aerobic growth conditions *in vitro*. A P5 catheter corresponding
196 to 61UP was also preserved in liquid N_2 after collection and grown anaerobically in rich media, As
197 reported (31), colonies were subjected to 16S rRNA and proteomic surveys and largely agreed
198 with the profiles derived from equivalent clinical samples. Lower abundance fastidious bacteria,
199 such as *Prevotella*, were identified by 16S rRNA sequence analysis from both clinical samples
200 and colony isolates. This supported the notion that microbes of low abundance in UP and CB
201 samples were not always in a detectable range for shotgun proteomics. Using frozen specimens
202 for colony isolation, only species that are viable during extended storage at -80˚C were identified.
203 This included *Serratia marcescens*, *K. pneumoniae*, *S. aureus*, and *E. faecalis* (Dataset S2,
204 Suppl. Data) all of which have cell walls encapsulated with protective exopolysaccharides. In
205 contrast, species that were quite abundant in some clinical specimens, *e.g. E. coli* and *A. urinae*,
206 were not isolated under these conditions.
207
208 Microbial proteins quantified by peptide-spectral counting from all UP and CB samples (Dataset
209 S4, Suppl. Data) were summed at species levels. One fungal species, *Candida albicans*, was
210 identified in P2 and P9 datasets at low levels. Common bacterial pathogens of the urinary tract
211 were more persistent in longitudinal profiles than rare pathogens and fastidious anaerobes (Fig.
212 3). *P. mirabilis* was dominant in samples from three patients with salt-encrusted CBs surveyed
213 over 3.5 to 5.5 months (P4, P6, and P7), but less so in P5 where salt encrustation was observed
214 for less than half of the samples. Both *P. stuartii* and *E. faecalis* persisted in two of the patient
215 sample series. Non-encrusted catheters (P1, P2, P8, and P9) were more dynamic in microbial
216 content of CBs over time. Most prevalent were *P. aeruginosa*, *E. coli* and *E. faecalis*. In the CBs of
217 P2 that followed three antibiotic treatment courses, *K. pneumoniae* was dominant. Among rare

pathogens, *Brevundimonas* (10UP-22UP), *Stenotrophomonas* (71CB), and *Acinetobacter* (5UP) colonized transiently, whereas *Bordetella hinzii* (10UP-33CB) and *S. marcescens* (15CB-50CB) displayed higher persistence over time. The box plots in Figure S5 (Suppl. Data) depict variances in bacterial species abundances comparing UP and CB proteomes in a patient-specific manner. No statistically significant differences in microbial composition for timepoint-matched UP and CB datasets were identified. This analysis suggests that the cycle of biofilm formation and dispersal occurs at the microbial community level. For the most part, UP samples contain those organisms that dispersed from CBs.

Proteomic data allow assessments of strains dominance and microbial adaptation to the catheter biofilm milieu.

Little is known about molecular adaptations of species to the complex microbial environment in CBs and the presence of the host's immune cells and their effectors at the catheter-urothelial interface. Furthermore, it was of interest to determine if specific strains of a microbial species were dominant in a series of samples from a given patient. We investigated these questions patient-specifically at the proteome level. Statistically significant abundance differences were identified for 664 bacterial proteins (ANOVA tests; Dataset S6, Suppl. Data). Interpreting all data is beyond this article's scope. We elaborate on *P. mirabilis*, *E. coli*, and *E. faecalis* because their proteomes were well-represented in datasets from several patients, with a focus on proteins relevant to bacterial energy metabolism and interactions with the host environment. HpmA was detected only in *P. mirabilis* proteomes pertaining to CBs of P7 (Fig. 4), supporting the notion that this putative hemolysin is expressed by few uropathogenic *P. mirabilis* strains. High abundance of HpmA in all P7 datasets suggests that a single *P. mirabilis* strain highly dominates the CB series of P7. A yersiniabactin-like iron/siderophore receptor (gene locus PMI2596) was abundant in the *P. mirabilis* proteomes of CB samples from P1 and P4, lower in abundance in P5 and absent in P6

and P7 samples (Fig. 4). The gene cluster for biosynthesis of yersiniabactin and expression of its receptor FyuA is considered part of the *E. coli* accessory genome. The abundances of the *E. coli* proteins FyuA and Irp1 (an enzyme encoded by one gene in this cluster) were also highly variant and most abundant in P1 and P2 datasets (Fig. 4). Some *E. coli* strains produce another siderophore, aerobactin, via the system IucA-D. Its receptor IutA (Fig. 4) and the L-lysine 6-monooxygenase IucD were differentially abundant in the *E. coli* proteomes of P1, P2, P5 and P8. Box plots displaying the variances of additional proteins involved in TMI uptake pathways among patients are included in Dataset S6 (Suppl. Data). In support of a single strain's dominance for a species in the CB series pertaining to a distinct patient, an *E. coli* plasmid-encoded ferric iron uptake system (UTI89_P010-P017) and the Hek adhesin factor were identified in multiple samples from P1 but not in those from any other patient.

We observed statistically significant abundance differences for bacterial proteins that contribute to fitness and survival in the human host, including the *P. mirabilis* MR/P fimbriae and the flagellin FliC (Fig. 4). The mannose-resistant fimbrial protein MrpA adheres to urothelial cells and catheters. FliC enables cell swarming and likely contributes to the pathogen's spread along catheter surfaces. MrpA was most abundant in P6, a case associated with very high CB biomasses and diagnosis of a renal infection. We identified differences in abundance for enzymes part of energy metabolism pathways in patient-specific proteome comparisons. The anaerobic respiration pathway Nar/Fdo (*P. mirabilis*), with nitrate as electron acceptor and formate as electron donor, was much more abundant in CBs from P6 than in CBs from other patients. NarG profiles are shown in Fig. 4. Abundance profiles were similar for SucA, a 2-oxoglutarate dehydrogenase subunit part of the citrate cycle. The citrate cycle produces reducing equivalents for nitrate reductase (Nar). Enzymes of the mixed acid fermentation (MAF) pathway were most abundant in CBs of P5, P7, and P8. The abundance profile of *P. mirabilis* formate C-

acetyltransferase (PflB) is depicted in Fig. 4. Aldehyde-alcohol dehydrogenases (AdhE) of *P. mirabilis* and *E. coli* were also differentially abundant (Dataset S6, Suppl. Data). Fittingly, fastidious bacteria were high biomass contributors only in samples from P5 (*A. massiliense* and *Propionimicrobium lymphophilium*) and P8 (*Campylobacter curvus* and *Veillonella parvula*). A fucose degradation pathway of *E. coli* appeared to be most active in P5 samples, with statistically significant differences in abundance for FucO, FucU and FucI. Lactaldehyde reductase FucI (Fig. 4) catalyzes the terminal step of anaerobic fucose metabolism. Many proteins with functional and structural roles in mRNA and protein biosynthesis (*P. mirabilis, E. coli*, and *E. faecalis*) had statistically significant abundance differences comparing the patient groups. In summary, the differential use of proteins and multi-molecular entities important to maintain the fitness of bacteria in biofilms (mobility, adhesion, energy metabolism), comparing CB series between patients, is indicative of adaptations influenced by host and microbial environments.

Functional correlations among molecular systems involved in TMI acquisition.

We assessed whether multi-subunit systems involved in TMI acquisition, often regulated by the iron starvation-sensing transcription factor Fur, positively correlated in expression levels. The proteomes of a subset of bacteria sharing CB niches (*E. faecalis*, *A. urinae*, *P. mirabilis*, and *E. coli*) in patients P1, P4, and P5 were targeted. Abundance correlation R-values of TMI acquisition systems derived from the individual patients' longitudinal CB timepoints were determined. There were no statistically significant correlations for P4 and P5 data. Strong positive correlations for *P. mirabilis*, *E. coli* and *E. faecalis* TMI acquisition systems, or proteins part of these systems, were observed for data from P1 (Fig. 5). These systems' abundances did not correlate with that of Fur itself, as shown for *P. mirabilis* Fur in Fig. 5. This transcription factor activates the expression of iron acquisition systems via a mechanism not dependent on its own abundance. The correlation analyses demonstrate that microbial cohabitants jointly respond to the starvation of iron and other

metal ions and express a versatile repertoire of proteins dedicated to their extracellular capture and import into the cell. The summed abundance of *P. mirabilis* ExbB and ExbD, subunits of the energy-transducing Ton system responsible for the proton motive force-dependent uptake of TMI/siderophores via TonB-dependent outer membrane receptors, positively correlated in abundance with the receptors they serve. MR/P fimbriae of *P. mirabilis* (MrpA-H) did not positively correlate in abundance with any TMI acquisition proteins. Three *E. faecalis* lipoproteins, subunits of ABC transporters predicted to bind TMIs, were expressed by the strains that cohabitated CBs of five patients: EF2076, EF0577, and EF3082. The abundances of EfaA (EF2076) varied comparing the *E. faecalis*-containing CB proteomes from five patients (Fig. 6A) and positively correlated with those of TMI acquisition systems of *P. mirabilis* and *E. coli* (Fig. 5). The data were similar for the sum of subunits of the ABC transporter (EfaABC). In a recent study, the system was found to be required for Mn^{2+} import and CAUTI pathogenesis (32). We expressed these *E. faecalis* lipoproteins recombinantly in *E. coli*, purified them, and determined protein melting profiles (T_m). Complex formation with small molecules, *e.g.* TMIs, stabilizes a protein and increases its T_m. We observed that purified EfaA and EF0577 had two T_m maxima in fluorescent dye-binding experiments. One T_m maximum appeared to represent an apoprotein binding a TMI as a cofactor. Denaturation eliminated this higher T_m peak, while renaturation in the presence of 50 µM $CoCl_2$ resulted in restitution of the high T_m maxima (Fig. 6). Protein melting profiles for EF3082 did not display two T_m peaks for any experimental condition. We infer that EfaA and EF0577 bind one or more TMIs and facilitate their ABC transport-mediated uptake into the *E. faecalis* cell.

Chronic innate immune responses result from persistent microbial colonization in all patients.

The absence of CAUTI symptoms in recurrently catheterized neurogenic bladder patients does not suggest absence of innate immune responses and pyuria (7, 28). Longitudinal human proteomic profiles allowed us to assess patient- and timepoint-specific quantitative differences in

the immune responses. First, we quantified relative protein abundances averaged from all 121 samples (Dataset S4, Suppl. Data). In Table 1, a subset of proteins with either a role in neutrophil- and eosinophil-mediated immune responses or as a cell biomarker is selected. Hemoglobin is a urine biomarker of tissue injury in the urethral and bladder mucosa. Hemoglobin subunits, *e.g.* HBB (Table 1), were moderately abundant in most datasets suggesting the occurrence of microhematuria in catheterized patients. High abundance of neutrophil-enriched and moderate abundance of eosinophil-enriched effector proteins (MPO, calgranulins and EPX, Table 1) suggest that both innate immune cell types infiltrated the urinary tract upon microbial colonization of the catheters. Based on a panel of cell-specific surface markers, as identified by the HCDM resource (33), granulocyte (CEACAM8) and neutrophil (CD177) markers were more abundant than B-cell, T-cell, macrophage and dendritic cell markers (Table 1). Urothelial umbrella cell surface markers were of very low abundance compared to keratins, consistent with the occurrence of squamous urothelial metaplasia and progressing epithelial cell keratinization due to chronic irritation of the patients' urinary tracts (34). Uroplakin-2 and KRT13 are included in Table 1. Complement system proteins such as C3 were also abundant, indicative of high activity of this innate immunity branch. Uromodulin, a protein forming polymerized gel-like aggregates in urine, is abundant regardless of immune cell infiltration and therefore served to normalize protein abundance for the quantitative analyses shown in Fig. 7.

Comparing datasets among the individual patients, we identified statistically significant variances in abundance for many proteins with functions in innate immunity (Figure S7, Suppl. Data). MPO and LTF data are depicted in Fig. 7A. MPO is the main ROS-generating enzyme in neutrophils. LTF is a multifunctional protein including an iron-sequestering function. Correlation analyses for numerous neutrophil and eosinophil effectors are displayed in Fig. 7B. This data shows that subsets of proteins cluster based on known enrichments in a specific type of cell or subcellular

organelle: for instance, the eosinophil granule proteins bone marrow proteoglycan PRG2 and EPX and, as reported in (35), azurophilic granule proteins released by neutrophils: MPO, cathepsin G, azurocidin, and elastase. Such correlation data support the notion that the effectors contribute to immune defenses triggered by persistent biofilm formation on catheters. Western blots for MPO, not normalized for total protein in UP samples, confirm activation of neutrophils in patients in response to CB formation. MPO blots for selected timepoints pertaining to three patients, shown in Fig. 7C (P2-6, P7-55, P4-47), revealed low band intensities. This is consistent with low UP/CB biomasses for these timepoints (Fig. 3). Regardless of patient origin, neutrophils infiltrate the urothelium and release their effectors at the catheter surfaces when they harbor microbial biofilms.

Antibiotic drug treatments influence composition and resilience of CBs, with instances of transient and permanent changes.

A wound infection of patient P7 was treated with Bactrim, a combination of sulfamethoxazol and trimethoprim (TMT), at timepoint 41UP/CB. This treatment was stopped a week prior to timepoint 56UP/CB, resulting in the transient bacterial elimination at timepoint UP/CB55. *P. mirabilis* rapidly recolonized as shown in Fig. 3. A cohabitant of the P7 CBs, *H. influenzae*, also recurred as a minor component at post-treatment timepoints. The virulence factor HpmA was highly abundant in the *P. mirabilis* proteome prior to and after treatment, supporting recurrence of colonization with the same *P. mirabilis* strain. Disk diffusion DSTs for a bacterial isolate (CB65) from P7 revealed that it was susceptible to a TMT/sulfonamide combination (Table 2). Treatment of P9 with levofloxacin over ten days resulted in reduced microbial biomass at timepoint UP/CB75 and eliminated *S. marcescens* from the biofilm (Fig. 3). But *E. faecalis* and *P. aeruginosa* strains persisted, and *S. aureus* and *C. albicans* emerged as new CB community members at post-treatment timepoints. Fungal pathogens are not inhibited by fluoroquinolone drugs. We also isolated a slowly growing *E. faecalis* strain on blood and Mueller-Hinton agar from 74CB. This

isolate was indeed resistant to a fluoroquinolone, ciprofloxacin (Table 2). *E. faecalis* has a high incidence of *parC* and *gyrA* mutations that confer fluoroquinolone resistance in strains causing UTI (36). We did not identify peptides displaying the common ParC and GyrA amino acid substitutions. A *S. marcescens* strain isolated from 74CB was susceptible to ciprofloxacin. We isolated a *S. aureus* strain from 75CB. This isolate was not only resistant to ciprofloxacin but also to ampicillin and cephaloxin, according to DSTs (Table 2). Several antibiotic drugs were administered to treat a P2 wound infection, with timepoints ranging from 10UP to 42CB (Fig. 3). Intravenous cephalosporin treatments eliminated strains of *S. aureus*, *E. faecalis*, *B. scardovii* and *P. aeruginosa* from the patient's catheters, while *Brevundimonas* and *Bordetella hinzii* strains were more resilient. Daptomycin treatment diminished the *B. hinzii* colonization burden, from 32CB to 33CB, and *K. pneumoniae* emerged as the dominant species. We did not test the *K. pneumoniae* isolate from 43CB for resistance to daptomycin, a last-resort antibiotic to treat Gram-positive infections, but DSTs revealed the strain's extended spectrum β-lactam and ciprofloxacin resistance (Table 2).

To gain further insights into antibiotic resistances of bacterial isolates observed in the DSTs, pan-proteome database searches including multiple genotypes for a species and ORFs derived from plasmids or pathogenicity islands were conducted. Thereby, database searches were expanded to "accessory proteomes". Bacteria harvested from DST plates and clinical samples were analyzed. Proteins linked to various modes of antibiotic resistance are listed in Dataset S8 (Suppl. Data). The *S. aureus* isolate from 75UP (P9) expressed the penicillin-binding protein 2 MecA, β-lactamase BlaZ and aminoglycoside 4'-adenylyltransferase AadD. Expression of the proteins matched the strain's reduced sensitivities to ampicillin, cephalexin and gentamycin, respectively. A *S. aureus* strain isolated from 53CB (P6), the patient diagnosed with a kidney infection, also expressed MecA. A *P. mirabilis* isolate from P6 (30CB) expressed aminoglycoside O-

phosphotransferase (APH(3')-Ia) and dihydrofolate reductase DfrA17, indicative of resistances to aminoglycosides and TMT, respectively. The *P. mirabilis* isolate from CB65 (P7) did not express these proteins. The *E. faecalis* isolate from 74UP expressed a dihydrofolate reductase (DfrE) and an aminoglycoside O-phosphotransferase (APH (3')-IIIa). DfrE expression explains the observed TMT resistance (Table 2). In summary, some bacterial pan-proteome analyses corroborated evidence of single- or multi-drug resistant species co-colonizing patient's catheters.

Discussion.

Our systems-level study on biofilms that grow on indwelling catheters of neurogenic bladder patients generates new insights into CB longitudinal dynamics. Meta-omics data demonstrate that dominant strains of distinct bacterial species recur in serially replaced catheters under challenge by the innate immune system and antibiotic drug treatments. Gaining these insights depends on clinical samples that CAUTI animal models cannot simulate. Such animal models cannot introduce the polymicrobial mixtures that human CBs are composed of. The range of micro- to anaerobic growth conditions that, we conclude, affect the CB profiles are impossible to mimic in CAUTI models. Culture-independent surveys identified many fastidious bacteria in CBs in the context of CAUTI and CAASB (22, 23, 37). We profiled strictly anaerobic bacteria cohabitating CBs in 6 of the 8 patients on the proteome level for the first time: *A. massiliense*, *P. lymphophilum*, *B. scardovii*, *V. parvula*, and *C. curvus*. Fastidious organisms more tolerant of oxygen (*A. urinae* and *G. sanguinis*) were identified as persistent colonizers of CBs. There is increasing awareness of the fact that such bacteria are more common causes of UTI and CAUTI in immunocompromised patients (38-40). The protection a biofilm offers makes it likely that such bacteria colonize hosts with functional immune systems. There is no evidence that the patients surveyed here, despite their spinal cord injuries, are immunocompromised. Animal models do not mimic the sequential replacement of catheters, a clinical need for many neurogenic bladder

418 patients, because of the one-time catheter implantation technique. Low quantities of biological
419 materials from murine catheters limit experiments requiring > 50 µL sample volumes (proteomics,
420 metabolomics). Differences of murine *vs.* human urothelial surface markers (18), Toll-like
421 receptors (41), cytokeratin abundance patterns in urothelial and stratified squamous epithelial
422 cells (42, 43), and the lack of key innate immune effectors in murine neutrophils (e.g. defensin-1)
423 encourage clinical investigations to study the crosstalk of polymicrobial biofilms with the host
424 immune system and to conceptualize new ideas for therapeutic interventions.

425 In partial agreement with studies in which microbial colonization of recurrently catheterized
426 patients was examined from UP samples (24, 25), we observed long-term bacteriuria for greater
427 than 90% of the specimens. In agreement with another survey of longitudinally profiled catheter
428 extracts (26), we observed frequent CB cohabitation by two or more pathogens and altered
429 microbial community profiles following antibiotic drug treatments. *P. mirabilis, K. pneumoniae, P.*
430 *aeruginosa, E. coli* and *E. faecalis* were most prevalent and persistent according to our data and
431 (26). In contrast to the cited studies, we found fastidious bacteria to be common CB cohabitants
432 derived from chronically catheterized patients. Spinal cord-injured cohorts, used in (25) and our
433 study, are not associated with any specific subset of uropathogens. We cannot confirm previous
434 reports where *P. stuartii* was found to be as common a cause of recurrent CAASB as *P. mirabilis*
435 (24, 25). Our data confirm that *P. mirabilis* strains have significant fitness advantages, resulting in
436 their persistence in and dominance of CBs, when catheters become encrusted with insoluble
437 phosphate salts and are used by the bacteria to establish co-aggregates with salts (3, 11, 12, 26).

438 Our UP and CB proteome data strongly support the notion that distinct strains of a given
439 microbe dominate the CB community of a given patient, as compared to a mixture of strains.
440 While absolute evidence to back up this claim requires analysis of the strains' genomes in a series
441 of CBs, which we plan to do in future work, identification of genes not part of a species' core

genome in some but not other patients allow this conclusion. For instance, HpmA, a *P. mirabilis* cytotoxin, was identified only in P7 samples. Nrp (PMI2596-PMI2605), a *P. mirabilis* siderophore biosynthesis system, was expressed only in P1 and P4, but not in samples from P5, P6, and P7. An *E. coli* plasmid-encoded ferric iron uptake system (UTI89_P010-P017) and adhesion factor Hek were consistently observed in P1 samples but absent in *E. coli* proteomes present in the CBs of other patients. The *E. coli* aerobactin biosynthesis system Iuc and its receptor IutA were abundant in P1, P2 and P5, but not present in samples from P8 and P9. Subunits of the twitching mobility type IV pilus were identified in CBs that *P. aeruginosa* contributed to in P1, but not in P2, P8, and P9 samples. The type IV pilus is part of the *P. aeruginosa* accessory genome and itself facilitates conjugative DNA transfer (44). The *E. coli* aerobactin system and the adhesin Hek were reported to be expressed by virulent strains that cause urosepsis (45) and neonatal meningitis (46), respectively. Nrp enzymes synthesize a yersiniabactin-like siderophore. Few *P. mirabilis* genomes have been sequenced and annotated so that insights into Nrp gene cluster frequency for clinical strains other than HI4320 (47) are not yet available. Patient-specific identifications of ORFs considered part of accessory genomes argue in favor of a single dominant genotype (strain) for a species. But it cannot be ruled out that other strains make minor contributions to the same CBs. Dominant strains re-colonize catheters that are replaced in patients, either from intracellular or extracellular urinary tract reservoirs. Intra-urothelial bacterial communities have been described for *E. coli* and *K. pneumoniae* (48, 49). Our data clearly support re-colonization at the community level given that the same species recur in longitudinal CB series. That, in turn, points towards extracellular retention of polymicrobial clusters dispersed from catheter surfaces and persisting in the urinary tract via mucosal adherence. Important adhesion proteins of Gram-negative bacteria in the urinary tract are fimbriae which varied in abundance in our datasets. Highly abundant were the MR/K fimbriae of *K. pneumoniae* (KPN03276-KPN03280 (50)) and MR/P fimbriae of *P. mirabilis* (PMI0263-PMI0270 (51)). The MrpA variance in abundance across datasets is displayed in Fig. 4.

Each species produced ECP-type fimbriae (KPN00290-KPN00295, PMI2997-3003), but in lower quantities. Fimbriae display phase variation and permit the rapid adaptation to conditions that foster resilience in the host milieu, including the attachment to biotic surfaces and medical devices (52, 53). Mannose-resistant MR/K and MR/P fimbriae, as well as the *P. aeruginosa* type IV pilus (54), are involved in cellular aggregation and biofilm formation. Consistent with our data and the literature, we conclude that these surface assemblies provide fitness advantages and mediate the persistence of strains that express them in the catheterized human urinary tract.

The proteomic data provided insights into the energy metabolism and transition metal acquisition of bacterial species simultaneously present in CBs derived from clinical samples, to our knowledge for the first time. The discussion focuses on *P. mirabilis, E. coli, and E. faecalis* because these bacteria formed mixed CB communities recurrently in several patients. Each species expressed at least two ABC transporters known or predicted to facilitate TMI import. The Gram-negative species expressed more than one biosynthesis system for siderophores and TonB-dependent receptors for their uptake when complexing Fe^{3+} and other TMIs. We assessed abundance correlations among the systems that facilitate TMI acquisition (Fig. 5). The correlations, derived from *P. mirabilis, E. coli,* and/or *E. faecalis* over a series of timepoints, were positive in CB profiles for P1, but not for P4 and P5. We hypothesize that these results reflect robust, simultaneous growth of the pathogens in P1. Growth requires TMI uptake in a metal ion-sequestering host milieu. TMIs are incorporated as cofactors or components of cofactors such as Fe-S and heme into enzymes that support metabolism in the cell, particularly energy metabolism. Several studies have established links between TMI acquisition in a TMI-starved host milieu and the expression levels of Fe and Fe-S cluster-harboring enzymes that support the bacterial energy metabolism (55, 56). Thus, we consider the observed correlation data supportive of active metabolism and growth in *P. mirabilis, E. coli,* and/or *E. faecalis* in P1. They may act cooperatively and competitively as it pertains to the uptake of TMIs (57). The cellular energy going into the

assembly of the TMI acquisition systems in the host environment appears to be high. For example, the *E. coli* strain in P1 highly expressed systems for aerobactin, yersiniabactin and enterobactin synthesis and uptake as well as heme uptake. Some of their components correlated with the abundance of the only characterized *E. faecalis* system for TMI acquisition, EfaABC. This ABC transporter is regulated by Mn^{2+} (58) and promotes bacterial growth under Mn^{2+} starvation conditions (32). Whether EfaABC can capture Mn^{2+} or other trace metals from *E. coli* or *P. mirabilis* siderophores or heme complexes remains to be shown. We expressed EfaA and another *E. faecalis* lipoprotein predicted to be part of an ABC transport system for TMIs (EF0577) recombinantly. Both proteins revealed biochemical evidence of Co^{2+} binding *in vitro*. An EfaA ortholog, PsaA, binds Mn^{2+} and Zn^{2+} ions but only transports Mn^{2+} into the *Streptococcus pneumoniae cell* (59). We hypothesize that the growth states of *P. mirabilis, E. coli,* and/or *E. faecalis* in P4 and P5 were variable, perhaps including different levels of quiescence, a known trait of persister cells in biofilms (60).

Furthermore, we hypothesize that communications among cohabitating bacteria affecting TMI homeostasis occur, a process that has been studied using model systems (57, 61). The human immune defense system perturbs this homeostasis. We surveyed proteins involved in sequestration of iron (LTF), zinc (calgranulins), and enterobactin (lipocalin-2). Like antimicrobial effectors such as the ROS-generating enzymes MPO and defensin-1, the proteins are released by neutrophils (or eosinophils) and abundant in human proteomes of UP and CB samples (Table 1). TMI-sequestering proteins starve bacteria of these essential cofactors at the CB-urothelial interface. At least three Gram-negative species profiled in CBs expressed high quantities of biosynthetic systems to produce lipocalin-2-insensitive siderophores: *P. aeruginosa* pyoverdin in P1, *E. coli* aerobactin in P1, P2 and P5, *E. coli* yersiniabactin in P1, P2, and P8; a *P. mirabilis* yersiniabactin-like siderophore in P1 and P4. Lipocalin-2 insensitivity likely increases the resilience of strains residing in CBs. Siderophore receptors operate in tandem with a TonB-

dependent energy-transducing system (TonB-ExbBD), which provides the energy for the transport of TMIs across the outer membrane. A single TonB energy-transducing system seems to be expressed by most Gram-negative bacteria, and the system's structure has been determined (62). TonB-ExbBD is an important molecular target to discover or design inhibitors. The system may disable TMI uptake in the human host when infections occur. Chemical compounds were screened to identify inhibitors of siderophore uptake using *E. coli* and *A. baumannii* TonB strains (63, 64). Such inhibitors have the potential to strengthen nutritional immunity and may be non-toxic in mammals given that TonB-ExbBD structures are unique to Gram-negative bacteria.

Finally, we observed different outcomes in three cases of systemic antibiotic treatments. Of note, the antibiotic drugs did not target microbial pathogens present in CBs, but those suspected to cause a comorbidity, chronic wounds. In P7, the *P. mirabilis* biofilm disappeared during Bactrim intake, but the strain regrew when antibiotic drug treatment was arrested. A CB isolate from this patient was sensitive to TMT/sulfanilamide treatment. In P9, a biofilm consisting of *E. faecalis, P. aeruginosa*, and *S. marcescens* was exposed to LEV treatment. This resulted in *S. marcescens* elimination from the biofilm. The other species persisted. *S. aureus* and *C. albicans* joined the reestablished biofilm. *E. faecalis* and *S. aureus* isolates from relevant CB timepoints were resistant to the fluoroquinolone CIP. P2 was treated sequentially with three different drugs over six weeks. Most pathogens were eliminated, but treatments failed to prevent sequential outgrowth of species not susceptible to the administered drugs, first *B. hinzii* (cephalosporin treatment), then an ESBL-resistant *K. pneumoniae* strain and *C. albicans* (daptomycin and fluoconazole treatments). Using pan-proteome searches for bacterial isolates grown *in vitro*, we identified proteins that cause antibiotic drug resistances in UTI and CAUTI pathogens, a serious public health problem threatening to lead to untreatable infections in the coming decades (65). The *S. aureus* strain from 75CB expressed BlaZ and MecA, proteins induced in expression via cross-talk among regulators of the corresponding genes (66). Additionally, the anoxic environment in deeper layers of biofilms

and quiescence allow bacteria to survive during drug treatments even if the genomes do not harbor specific antibiotic resistance genes or drug efflux pumps (60). CAASB in chronically catheterized patients is a difficult medical problem. This study highlights the microbial escape routes and adaptability of polymicrobial communities formed on a medical device in the human body, following exposure to antibiotic drugs, nutritional starvation (e.g. oxygen and TMIs) and antimicrobial effectors of the immune system.

Methods

Ethics Statement.

The Southwest Regional Wound Care Center (SRWCC) in Lubbock, Texas, and the J. Craig Venter Institute (JCVI, Rockville, Maryland) created a human subject protocol and a study consent form (#56-RW-022), which were approved by the Western Institutional Review Board (WIRB) in Olympia, Washington, followed by JCVI's IRB in 2013. All human subjects were adults and provided written consent. The specimens were collected firsthand for the purpose of this study. There was a medical need to serially replace indwelling Foley catheters in patients due to their affliction with neurogenic bladder syndrome. Scientists at the JCVI did not have access to data allowing patient identification. Medical metadata for the subjects were encrypted. Electronic and printed medical records at the clinical site were retained for 4 years to facilitate the integration of medical and molecular research data.

Human subjects and study design.

Nine human subjects enrolled in this prospective study. They had irreversible spinal cord injuries (SCIs) and suffered from neurogenic bladder syndrome. Catheter replacement was part of routine patient care at SRWCC. Medical data included gender, ethnicity, antibiotic use, diagnosis of chronic wound infections, and diabetes. Facilitated by medical staff, the enrolled subjects provided

3 to 15 specimens (urethral catheters and urine from catheter collection bags) collected longitudinally at the clinic in 1- to 4-week intervals, depending on the number of visits that patients and physician agreed upon. Catheters were cut into 1-inch pieces, placed in polypropylene tubes and stored at -20˚C, minimizing external contamination by use of gloves and sterile razor blades. Urine samples were obtained from catheter bag ports swabbed clean with alcohol prior to collection. Urine aliquots of 20 to 50 ml were stored at -20˚C. Infrequent draining of catheter bags may have allowed some *ex vivo* microbial growth in urine specimens. We assume that the quantitative ratios of microbes in urine sediments on the collection dates do not reflect those in the urine excreted over time. Containers in which specimens were stored were kept frozen during transport and transferred to a -80˚C freezer until further use at JCVI.

Urine and catheter specimen extraction and protein solubilization for proteomics.

The catheter materials were latex in the case of 8 patients and silicone (patient P7). The pH, color and turbidity of urine specimens and the crystallization of salts inside and on the surface of catheter segments were noted. To obtain a urine pellet (UP) from a sample, an aliquot was thawed, adjusted to 20˚C and, if acidic, neutralized with 1 M Tris-HCl (pH 8.1) to a pH of ~ 6.5 to 7.5, and centrifuged at 3,200 × g for 15 minutes. UPs were aliquoted for rDNA and protein extractions and spare samples in ratios of approximately 10%, 45% and 45%, respectively. Urethral catheter pieces were extracted in two steps. Submerged in 100 mM sodium acetate (pH 5.5), 20 mM sodium meta-periodate, and 300 mM NaCl, catheter pieces were agitated in an ultrasonic water bath for 10 min at 20˚C. The supernatant was recovered and concentrated. This was followed by two solubilization cycles of the pellet with a denaturing SED solution (1% SDS (v/v), 5 mM EDTA and 50 mM DTT) including 3 min heat treatment at 95˚C. Two supernatants were recovered that we termed CB-1 (Na-acetate buffer) and CB-2 (SED solution). The extraction of UP samples was limited to solubilization in SED solution. Experimental details were described

592 previously (28, 31). All centrifugal centrifugation steps were performed using Ultrafree-4 filter units
593 (10 kDa MWCO), potentially eliminating small peptides from the concentrates. However, we
594 determined that peptides with M_r values lower than 5 kDa (e.g. neutrophil defensin-1; 3-4 kDa)
595 were partially retained. Processing steps for the solubilized UP and CB samples were based on
596 the Filter-Aided Sample Preparation (FASP) method (67), adapted by us to the use of 100 µg
597 protein for digestion with sequencing-grade trypsin in 50:1 ratios in Vivacon 10k filters (Sartorius
598 AG, Germany) (28). FASP-processed peptide mixtures were desalted using the Stage-Tip method
599 (68) and lyophilized for LC-MS/MS proteomic analysis.
600
601 *Shotgun proteomics via LC-MS/MS.*
602 Desalted peptide mixtures derived from UP, CB-1, and CB-2 samples were dissolved in 10 µl
603 0.1% formic acid (solvent A) and analyzed using one of two LC-MS/MS systems: (1) a high-
604 resolution Q-Exactive mass spectrometer (MS) coupled to an Ultimate 3000-nano LC system; (2)
605 a low-resolution LTQ-Velos Pro ion-trap mass spectrometer coupled to an Easy-nLC II system.
606 Both systems (Thermo Scientific, San Jose, CA) were equipped with a FLEX nano-electrospray
607 ion source at the LC-MS interface. Analytic procedures were previously described for the Q-
608 Exactive (69, 70) and LTQ-Velos Pro (71) platforms. For LTQ-Velos Pro analysis, peptides present
609 in a sample were trapped on a C_{18} trap column (100 µm × 2 cm, 5 µm pore size, 120 Å) and
610 separated on a PicoFrit C_{18} analytical column (75 µm × 15 cm, 3 µm pore size, 150 Å) at a flow
611 rate of 200 nl/min. Starting with solvent A, a linear gradient from 10% to 30% solvent B (0.1%
612 formic acid in acetonitrile) over 195 minutes was followed by a linear gradient from 30% to 80%
613 solvent B over 20 min and re-equilibration with solvent A for 5 min. Following each sample, the
614 columns were washed thrice using a 30-min solvent A to B linear gradient elution to avoid sample
615 carry-over. For Q-Exactive analysis, LC was conducted as reported earlier (69). Electrospray
616 ionization was achieved by applying 2.0 kV distally via a liquid junction. Parallel to LC gradient

617 elution, peptide ions were analyzed in a MS^1 data-dependent mode to select ions for MS^2 scans
618 using the software application XCalibur *v2.2* (Thermo Scientific). The fragmentation modes were
619 collision-induced dissociation (CID) with a normalized collision energy of 35% (LTQ-Velos Pro)
620 and higher-energy collisional dissociation (HCD) with a normalized collision energy of 27% (Q-
621 Exactive). Dynamic exclusion was enabled. MS^2 ion scans for the same MS^1 *m/z* value were
622 repeated once and then excluded from further analysis for 30s. Survey (MS^1) scans ranged from a
623 *m/z* range of 380 to 1,800 followed by MS^2 scans for selected precursor ions. Survey scans with
624 the Q-Exactive were acquired at a resolution of 70,000 (m/Δm) with a *m/z* range from 250 to
625 1,800. MS^2 scans were performed at a resolution of 17,500. The ten most intense ions were
626 fragmented in each cycle. Ions that were unassigned or had a charge of +1 were rejected from
627 further analysis. Two or three technical LC-MS/MS replicates were run for UP, CB-1 and CB-2
628 peptide extracts.
629
630 *Computational proteomic data analyses and proteome quantifications.*
631 The raw MS files were combined for database searches as follows: (1) all technical replicates for a
632 given UP sample; (2) all replicates from both CB-1 and CB-2 fractions for a given CB sample. The
633 Sequest HT algorithm integrated in the software tool Proteome Discoverer v1.4 (Thermo
634 Scientific) was used as the search engine with analytical parameters described previously (69,
635 70). Only rank-1 peptides with a length of at least seven amino acids were considered. The FDR
636 rates were estimated using the integrated Percolator tool with a (reverse sequence) decoy
637 database. Protein hits identified with a 1% FDR threshold were accepted for data interpretation.
638 The 'protein grouping' function was enabled to ensure that only one protein was reported when
639 multiple proteins shared a set of identified peptides. The database contents were the reviewed
640 protein sequence entries in the non-redundant Human UniProt database (release 2015-16; 20,195
641 sequences) and sequence entries for 23 microbial genomes reported as major causes of UTI (69).

Based on 16S rRNA genus assignments and iterative proteomic searches using database subsets for distinct species part of the same genus, the proteomic searches were customized for the same series from each patient. Iterative searches followed by database customization were also applied to samples containing one or potentially more members of the Enterobacteriaceae family. The entire list of species searched in this process is listed in Table S3 (Suppl. Data). The pan-proteome database searches for five distinct microbial species were performed by downloading non-redundant pan-proteome sequence databases from UniProt-Proteome using the Sequest HT algorithm as mentioned above. MS raw files were deposited in PRIDE (via ProteomeXchange) with the identifier PXD012048. The sums of peptide-spectral match counts (PSMs) assigned to each microbial species and *Homo sapiens* were the basis for the individual species-based quantification in both UP and CB samples. Relative to the total proteome (all PSMs) in a dataset, normalized abundance values were obtained for all species in the Proteome Discoverer v1.4-derived dataset. They were the basis of quantitative displays in Fig. 3 and Figure S5 (Suppl. Data). For quantitative analyses that assessed protein variances, of human and microbial species origins, normalization was based on total PSMs of the respective species. This normalization pertains to proteomic data displayed in Figs. 4, 5, 6 and 7, Table 1, Dataset S6 and Figure S7.

Microbiota analyses.

Microbial cell lysis and DNA extraction methods from catheter extracts and UP samples (31) and the amplification of V1-V3 regions of the 16S rDNA bacterial genes as well as sequencing on the MiSeq sequencer from Illumina Inc. were described previously (72). The UPARSE pipeline for the phylogenetic analysis was used (73). OTUs were generated *de novo* from raw sequence reads using default parameters in UPARSE, the Wang classifier and bootstrapping using 100 iterations. The taxonomies were assigned to the OTUs using Mothur and applying the SILVA 16S rRNA database version 123 as reference database (74). Unbiased, metadata-independent filtering was

667 applied at each level of the taxonomy by eliminating samples with less than 2000 reads and OTUs
668 present in less than ten samples. Filtered data were analyzed based on the relative contributions
669 of microbial genera in a distinct sample. The Shannon index was used to measure the alpha
670 diversity.
671
672 *Microbial cultures.*
673 Surviving bacteria present in frozen catheter extracts and UP samples stored at -80˚C were
674 cultured on BHI broth, blood and MacConkey agar plates to isolate strains. Single colonies were
675 picked, Gram-stained and microscopically assessed before culture stocks were generated either
676 directly from a plate or a 5-10 mL overnight BHI suspension culture. Stocks were frozen in 10%
677 glycerol at -80˚C. To determine the identity of bacterial species, cell lysis, proteomic sample
678 processing and database search methods we mentioned in the context of clinical sample analysis
679 were used. If a dataset suggested impurities, bacterial strains were streaked out again from the
680 original stock and new colonies were picked and reanalyzed. The OD_{600} values reached for *E.*
681 *faecalis* strains in BHI media were below 0.6, the values for species of the Enterobacteriaceae
682 family were usually higher than 0.8. Some fastidious bacterial species were isolated and lysed
683 directly from blood agar plates for proteomic analysis. The isolation of other fastidious bacteria
684 derived from anaerobic storage in liquid nitrogen and anaerobic culture, without freezing catheter
685 specimens, was previously reported (31). Further details are provided in Dataset S2 (Suppl. Data).
686
687 *Expression vectors, gene cloning, and recombinant protein expression.*
688 Two expression vectors were used to clone EF2076, EF0577 and EF3082 (*E. faecalis* V583) into
689 the *E. coli* strain BL21(DE3)/pMagic (75). The ccdB cassette was inserted into the cloning region
690 to enhance the efficiency of screening for the correct clone. pMCSG53 encodes the N-terminal
691 His-tag (75). PCR primers in Table 3 were used to amplify the ORFs excluding export signal

692 sequences. Inserted DNA fragments were prepared using standard PCR protocols using Phusion
693 polymerase (New England Biolabs). The pMCSG53 vector was linearized by cleavage of the
694 cloning site with SspI, and PCR products were cloned using the Gibson Assembly method (76)
695 and transformed into *E. coli* DH5α. Sequences of the clones were validated by Sanger
696 sequencing. Their transformation into BL21(DE3)/pMagic was followed by growth at 37 °C in 0.5 L
697 LB containing 100 µg/ml ampicillin to an OD_{600} of ~ 0.8 when expression was induced by adding 1
698 mM IPTG. Following incubation at 20°C for 16-18 hours, the cells were lysed. *E. faecalis* target
699 proteins were purified on Ni-NTA resin, cleaving the affinity tags with TEV protease as previously
700 reported (77). Purity and solubility of the purified proteins was assessed by Nu-PAGE.
701
702 *Thermal shift assay.*
703 Interaction of proteins with a small molecule can increase its stability and the melting temperature
704 (T_m) (78). To denature each of the purified *E. faecalis* proteins, a 1 mg/ml solution was incubated
705 with 1 ml 6 M guanidine-HCl (pH 8). To renature the protein, 50 µl Ni-NTA agarose resin was
706 added. The suspension was incubated gently agitating at 4°C for 1 h. The flow-through fraction
707 was discarded. The resin was washed with 8 M urea/PBS, and the protein gradually renatured via
708 buffer exchange into PBS followed by elution in 50 µl of an elution buffer containing 250 mM
709 imidazole. Renatured proteins were either left in PBS or $CoCl_2$ was added at a final concentration
710 of 50 µM. Ten µl of a protein preparation (0.5 mg/ml) was placed in a 384-well plate adding 2 µl
711 100X SYPRO Orange. Temperature melting profiles were monitored in a Light Cycler 480 (Roche
712 Life Science).
713
714 *Disk diffusion antibiotic drug susceptibility tests.*
715 We followed guidelines from a Manual of Antimicrobial Susceptibility Testing (79) to perform drug
716 susceptibility tests via disk diffusion. All antibiotics were dissolved as specified by the Korean

717 society of laboratory medicine manual and placed on 0.6 mm disks in concentrations as follows:
718 Ampicillin (100 µg); Cefotaxime (30 µg); Cephalexin (30 µg); Ciprofloxacin (5 µg);
719 Sulfanilamide/TMT (200µg/ 12µg); and Gentamycin (30 µg). The McFarland standard (0.5) was
720 used to adjust bacterial turbidity and plate approximately 1.5 X 10^8 CFU/ml of bacterial inoculum
721 from a ~ 6h BHI culture (Gram-negative) or a Mueller-Hinton agar plate (Gram-positive).
722 Clearance zones were measured after 16 hours of growth at 37˚C in a 5% CO_2 incubator.
723
724 *Statistical analysis methods.*
725 To determine statistical changes in taxonomic α-diversity, Wilcoxon rank sum tests were
726 performed. These tests were also used to assess variation in the abundances of proteins in
727 proteomic datasets from different patients. Analysis of variance (ANOVA) was used to compare
728 the variation between patients. We applied a P-value cutoff of 0.05 to determine statistically
729 significance. The correlation plot was derived from the corrplot package in R, using the Pearson
730 correlation with a P-value less than 0.05. Box plots with statistically significance data were
731 generated using ggsignify and ggplots in R.
732
733 ## Acknowledgements
734 This work was supported by the National Institutes of Health grant R01GM103598 titled “Urethral
735 catheter-associated polybacterial biofilm formation and dispersal”. The funder had no role in study
736 design, data collection and interpretation, or decisions to submit the work for publication. We
737 thank the Ruggles Family Foundation for the support in acquiring the Q-Exactive mass
738 spectrometer.
739
740 ## References
741 1. Foxman B. 2010. The epidemiology of urinary tract infection. Nat Rev Urol 7:653-60.

2. Saint S, Chenoweth CE. 2003. Biofilms and catheter-associated urinary tract infections. Infect Dis Clin North Am 17:411-32.

3. Stickler DJ. 2008. Bacterial biofilms in patients with indwelling urinary catheters. Nat Clin Pract Urol 5:598-608.

4. Flores-Mireles AL, Walker JN, Caparon M, Hultgren SJ. 2015. Urinary tract infections: epidemiology, mechanisms of infection and treatment options. Nat Rev Microbiol 13:269-84.

5. Macleod SM, Stickler DJ. 2007. Species interactions in mixed-community crystalline biofilms on urinary catheters. J Med Microbiol 56:1549-57.

6. Majumder MI, Ahmed T, Hossain D, Begum SA. 2014. Bacteriology and antibiotic sensitivity patterns of urinary tract infections in a tertiary hospital in Bangladesh. Mymensingh Med J 23:99-104.

7. Hooton TM, Bradley SF, Cardenas DD, Colgan R, Geerlings SE, Rice JC, Saint S, Schaeffer AJ, Tambayh PA, Tenke P, Nicolle LE. 2010. Diagnosis, prevention, and treatment of catheter-associated urinary tract infection in adults: 2009 International Clinical Practice Guidelines from the Infectious Diseases Society of America. Clin Infect Dis 50:625-63.

8. Boucher HW, Talbot GH, Bradley JS, Edwards JE, Gilbert D, Rice LB, Scheld M, Spellberg B, Bartlett J. 2009. Bad bugs, no drugs: no ESKAPE! An update from the Infectious Diseases Society of America. Clin Infect Dis 48:1-12.

9. Nielubowicz GR, Mobley HL. 2010. Host-pathogen interactions in urinary tract infection. Nat Rev Urol 7:430-41.

10. Weichhart T, Haidinger M, Horl WH, Saemann MD. 2008. Current concepts of molecular defence mechanisms operative during urinary tract infection. Eur J Clin Invest 38 Suppl 2:29-38.

11. Norsworthy AN, Pearson MM. 2017. From Catheter to Kidney Stone: The Uropathogenic Lifestyle of Proteus mirabilis. Trends Microbiol 25:304-315.

12. Schaffer JN, Pearson MM. 2015. Proteus mirabilis and Urinary Tract Infections. Microbiol Spectr 3.

13. Haraoka M, Hang L, Frendeus B, Godaly G, Burdick M, Strieter R, Svanborg C. 1999. Neutrophil recruitment and resistance to urinary tract infection. J Infect Dis 180:1220-9.

14. Yu Y, Kwon K, Tsitrin T, Bekele S, Sikorski P, Nelson KE, Pieper R. 2017. Characterization of Early-Phase Neutrophil Extracellular Traps in Urinary Tract Infections. PLoS Pathog 13:e1006151.

15. Yu Y, Sikorski P, Smith M, Bowman-Gholston C, Cacciabeve N, Nelson KE, Pieper R. 2017. Comprehensive Metaproteomic Analyses of Urine in the Presence and Absence of Neutrophil-Associated Inflammation in the Urinary Tract. Theranostics 7:238-252.

16. Hannan TJ, Roberts PL, Riehl TE, van der Post S, Binkley JM, Schwartz DJ, Miyoshi H, Mack M, Schwendener RA, Hooton TM, Stappenbeck TS, Hansson GC, Stenson WF, Colonna M, Stapleton AE, Hultgren SJ. 2014. Inhibition of Cyclooxygenase-2 Prevents Chronic and Recurrent Cystitis. EBioMedicine 1:46-57.

17. Schreiber HLt, Conover MS, Chou WC, Hibbing ME, Manson AL, Dodson KW, Hannan TJ, Roberts PL, Stapleton AE, Hooton TM, Livny J, Earl AM, Hultgren SJ. 2017. Bacterial virulence phenotypes of Escherichia coli and host susceptibility determine risk for urinary tract infections. Sci Transl Med 9.

18. Wu XR, Kong XP, Pellicer A, Kreibich G, Sun TT. 2009. Uroplakins in urothelial biology, function, and disease. Kidney Int 75:1153-65.

19. Nielubowicz GR, Smith SN, Mobley HL. 2010. Zinc uptake contributes to motility and provides a competitive advantage to Proteus mirabilis during experimental urinary tract infection. Infect Immun 78:2823-33.

20. Subashchandrabose S, Mobley HL. 2015. Back to the metal age: battle for metals at the host-pathogen interface during urinary tract infection. Metallomics 7:935-42.

21. Sabir N, Ikram A, Zaman G, Satti L, Gardezi A, Ahmed A, Ahmed P. 2017. Bacterial biofilm-based catheter-associated urinary tract infections: Causative pathogens and antibiotic resistance. Am J Infect Control 45:1101-1105.

22. Frank DN, Wilson SS, St Amand AL, Pace NR. 2009. Culture-independent microbiological analysis of foley urinary catheter biofilms. PLoS One 4:e7811.

794 23. Xu Y, Moser C, Al-Soud WA, Sorensen S, Hoiby N, Nielsen PH, Thomsen TR. 2012. Culture-
795 dependent and -independent investigations of microbial diversity on urinary catheters. J Clin
796 Microbiol 50:3901-8.
797 24. Warren JW, Tenney JH, Hoopes JM, Muncie HL, Anthony WC. 1982. A prospective microbiologic
798 study of bacteriuria in patients with chronic indwelling urethral catheters. J Infect Dis 146:719-23.
799 25. Dedeic-Ljubovic A, Hukic M. 2009. Catheter-related urinary tract infection in patients suffering from
800 spinal cord injuries. Bosn J Basic Med Sci 9:2-9.
801 26. Mathur S, Suller MT, Stickler DJ, Feneley RC. 2006. Prospective study of individuals with long-term
802 urinary catheters colonized with Proteus species. BJU Int 97:121-8.
803 27. Rousseau M, Goh HM, Holec S, Albert ML, Williams RB, Ingersoll MA, Kline KA. 2016. Bladder
804 catheterization increases susceptibility to infection that can be prevented by prophylactic antibiotic
805 treatment. JCI Insight 1:e88178.
806 28. Yu Y, Zielinski M, Rolfe M, Kuntz M, Nelson H, Nelson KE, Pieper R. 2015. Similar Neutrophil-
807 Driven Inflammatory and Antibacterial Activities for Symptomatic and Asymptomatic Bacteriuria in
808 Elderly Patients. Infect Immun doi:IAI.00745-15 [pii]
809 10.1128/IAI.00745-15.
810 29. Jones BD, Mobley HL. 1987. Genetic and biochemical diversity of ureases of Proteus, Providencia,
811 and Morganella species isolated from urinary tract infection. Infect Immun 55:2198-203.
812 30. Moustafa A, Li W, Singh H, Moncera KJ, Torralba MG, Yu Y, Manuel O, Biggs W, Venter JC,
813 Nelson KE, Pieper R, Telenti A. 2018. Microbial metagenome of urinary tract infection. Sci Rep
814 8:4333.
815 31. Yu Y, Tsitrin T, Singh H, Doerfert SN, Sizova MV, Epstein SS, Pieper R. 2018. Actinobaculum
816 massiliense Proteome Profiled in Polymicrobial Urethral Catheter Biofilms. Proteomes 6.
817 32. Colomer-Winter C, Flores-Mireles AL, Baker SP, Frank KL, Lynch AJL, Hultgren SJ, Kitten T,
818 Lemos JA. 2018. Manganese acquisition is essential for virulence of Enterococcus faecalis. PLoS
819 Pathog 14:e1007102.

33. Council H. 2010. Human Cell Differentiation Molecules abstr 9th International Conference on Human Leukocyte Differentiation Antigens (HLDA9) Barcelona, 11-13 March 2010. HCDM Council (Human Cell Differentiation Molecules, Copyright © 2016),

34. Liang FX, Bosland MC, Huang H, Romih R, Baptiste S, Deng FM, Wu XR, Shapiro E, Sun TT. 2005. Cellular basis of urothelial squamous metaplasia: roles of lineage heterogeneity and cell replacement. J Cell Biol 171:835-44.

35. Lominadze G, Powell DW, Luerman GC, Link AJ, Ward RA, McLeish KR. 2005. Proteomic analysis of human neutrophil granules. Mol Cell Proteomics 4:1503-21.

36. Yasufuku T, Shigemura K, Shirakawa T, Matsumoto M, Nakano Y, Tanaka K, Arakawa S, Kawabata M, Fujisawa M. 2011. Mechanisms of and risk factors for fluoroquinolone resistance in clinical Enterococcus faecalis isolates from patients with urinary tract infections. J Clin Microbiol 49:3912-6.

37. Fouts DE, Pieper R, Szpakowski S, Pohl H, Knoblach S, Suh M-J, Huang S-T, Ljungberg I, Sprague BM, Lucas SK, Torralba M, Nelson KE, Groah SL. 2012. Integrated next-generation sequencing of 16S rDNA and metaproteomics differentiate the healthy urine microbiome from asymptomatic bacteriuria in neuropathic bladder associated with spinal cord injury. Journal of Translational Medicine 10:174-174.

38. Lotte R, Lotte L, Ruimy R. 2016. Actinotignum schaalii (formerly Actinobaculum schaalii): a newly recognized pathogen-review of the literature. Clin Microbiol Infect 22:28-36.

39. Takahashi S, Xu C, Sakai T, Fujii K, Nakamura M. 2018. Infective endocarditis following urinary tract infection caused by Globicatella sanguinis. IDCases 11:18-21.

40. Zhang Q, Kwoh C, Attorri S, Clarridge JE, 3rd. 2000. Aerococcus urinae in urinary tract infections. J Clin Microbiol 38:1703-5.

41. Mestas J, Hughes CCW. 2004. Of mice and not men: differences between mouse and human immunology. Journal of immunology (Baltimore, Md : 1950) 172:2731-8.

42. Laguna P, Smedts F, Nordling J, Horn T, Bouchelouche K, Hopman A, de la Rosette J. 2006. Keratin expression profiling of transitional epithelium in the painful bladder syndrome/interstitial cystitis. Am J Clin Pathol 125:105-10.

43. Vaidyanathan S, McDicken IW, Ikin AJ, Mansour P, Soni BM, Singh G, Sett P. 2002. A study of cytokeratin 20 immunostaining in the urothelium of neuropathic bladder of patients with spinal cord injury. BMC Urol 2:7.

44. Kung VL, Ozer EA, Hauser AR. 2010. The accessory genome of Pseudomonas aeruginosa. Microbiol Mol Biol Rev 74:621-41.

45. Johnson JR, Moseley SL, Roberts PL, Stamm WE. 1988. Aerobactin and other virulence factor genes among strains of Escherichia coli causing urosepsis: association with patient characteristics. Infect Immun 56:405-12.

46. Fagan RP, Smith SG. 2007. The Hek outer membrane protein of Escherichia coli is an auto-aggregating adhesin and invasin. FEMS Microbiol Lett 269:248-55.

47. Himpsl SD, Pearson MM, Arewang CJ, Nusca TD, Sherman DH, Mobley HL. 2010. Proteobactin and a yersiniabactin-related siderophore mediate iron acquisition in Proteus mirabilis. Mol Microbiol 78:138-57.

48. Rosen DA, Hooton TM, Stamm WE, Humphrey PA, Hultgren SJ. 2007. Detection of intracellular bacterial communities in human urinary tract infection. PLoS Med 4:e329.

49. Rosen DA, Pinkner JS, Jones JM, Walker JN, Clegg S, Hultgren SJ. 2008. Utilization of an intracellular bacterial community pathway in Klebsiella pneumoniae urinary tract infection and the effects of FimK on type 1 pilus expression. Infect Immun 76:3337-45.

50. Murphy CN, Mortensen MS, Krogfelt KA, Clegg S. 2013. Role of Klebsiella pneumoniae type 1 and type 3 fimbriae in colonizing silicone tubes implanted into the bladders of mice as a model of catheter-associated urinary tract infections. Infect Immun 81:3009-17.

51. Zhao H, Li X, Johnson DE, Blomfield I, Mobley HL. 1997. In vivo phase variation of MR/P fimbrial gene expression in Proteus mirabilis infecting the urinary tract. Mol Microbiol 23:1009-19.

871 52. Jacobsen SM, Stickler DJ, Mobley HL, Shirtliff ME. 2008. Complicated catheter-associated urinary
872 tract infections due to Escherichia coli and Proteus mirabilis. Clin Microbiol Rev 21:26-59.
873 53. van der Woude MW, Baumler AJ. 2004. Phase and antigenic variation in bacteria. Clin Microbiol
874 Rev 17:581-611, table of contents.
875 54. O'Toole GA, Kolter R. 1998. Flagellar and twitching motility are necessary for Pseudomonas
876 aeruginosa biofilm development. Mol Microbiol 30:295-304.
877 55. Miller HK, Auerbuch V. 2015. Bacterial iron-sulfur cluster sensors in mammalian pathogens.
878 Metallomics 7:943-56.
879 56. Pieper R, Fisher CR, Suh MJ, Huang ST, Parmar P, Payne SM. 2013. Analysis of the proteome of
880 intracellular Shigella flexneri reveals pathways important for intracellular growth. Infect Immun
881 81:4635-48.
882 57. Griffin AS, West SA, Buckling A. 2004. Cooperation and competition in pathogenic bacteria. Nature
883 430:1024-7.
884 58. Low YL, Jakubovics NS, Flatman JC, Jenkinson HF, Smith AW. 2003. Manganese-dependent
885 regulation of the endocarditis-associated virulence factor EfaA of Enterococcus faecalis. J Med
886 Microbiol 52:113-9.
887 59. Dintilhac A, Alloing G, Granadel C, Claverys JP. 1997. Competence and virulence of Streptococcus
888 pneumoniae: Adc and PsaA mutants exhibit a requirement for Zn and Mn resulting from inactivation
889 of putative ABC metal permeases. Mol Microbiol 25:727-39.
890 60. Lewis K. 2010. Persister cells. Annu Rev Microbiol 64:357-72.
891 61. Harrison F, Buckling A. 2009. Siderophore production and biofilm formation as linked social traits.
892 ISME J 3:632-4.
893 62. Celia H, Noinaj N, Zakharov SD, Bordignon E, Botos I, Santamaria M, Barnard TJ, Cramer WA,
894 Lloubes R, Buchanan SK. 2016. Structural insight into the role of the Ton complex in energy
895 transduction. Nature 538:60-65.

63. Nairn BL, Eliasson OS, Hyder DR, Long NJ, Majumdar A, Chakravorty S, McDonald P, Roy A, Newton SM, Klebba PE. 2017. Fluorescence High-Throughput Screening for Inhibitors of TonB Action. J Bacteriol 199.

64. Yep A, McQuade T, Kirchhoff P, Larsen M, Mobley HL. 2014. Inhibitors of TonB function identified by a high-throughput screen for inhibitors of iron acquisition in uropathogenic Escherichia coli CFT073. MBio 5:e01089-13.

65. Mazzariol A, Bazaj A, Cornaglia G. 2017. Multi-drug-resistant Gram-negative bacteria causing urinary tract infections: a review. J Chemother 29:2-9.

66. Arede P, Ministro J, Oliveira DC. 2013. Redefining the role of the beta-lactamase locus in methicillin-resistant Staphylococcus aureus: beta-lactamase regulators disrupt the MecI-mediated strong repression on mecA and optimize the phenotypic expression of resistance in strains with constitutive mecA expression. Antimicrob Agents Chemother 57:3037-45.

67. Wisniewski JR, Zougman A, Nagaraj N, Mann M. 2009. Universal sample preparation method for proteome analysis. Nat Methods 6:359-62.

68. Yu Y, Smith M, Pieper R. 2014. A spinnable and automatable StageTip for high throughput peptide desalting and proteomics. Protocol Exchange. doi:10.1038/protex.2014.1033(doi:doi:10.1038/protex.2014.1033.

69. Yu Y, Sikorski P, Bowman-Gholston C, Cacciabeve N, Nelson KE, Pieper R. 2015. Diagnosing inflammation and infection in the urinary system via proteomics. J Transl Med 13:111.

70. Yu Y, Suh MJ, Sikorski P, Kwon K, Nelson KE, Pieper R. 2014. Urine sample preparation in 96-well filter plates for quantitative clinical proteomics. Anal Chem 86:5470-7.

71. Suh MJ, Tovchigrechko A, Thovarai V, Rolfe MA, Torralba MG, Wang J, Adkins JN, Webb-Robertson BJ, Osborne W, Cogen FR, Kaplowitz PB, Metz TO, Nelson KE, Madupu R, Pieper R. 2015. Quantitative Differences in the Urinary Proteome of Siblings Discordant for Type 1 Diabetes Include Lysosomal Enzymes. J Proteome Res 14:3123-35.

72. Singh H, Yu Y, Suh MJ, Torralba MG, Stenzel RD, Tovchigrechko A, Thovarai V, Harkins DM, Rajagopala SV, Osborne W, Cogen FR, Kaplowitz PB, Nelson KE, Madupu R, Pieper R. 2017.

923 Type 1 Diabetes: Urinary Proteomics and Protein Network Analysis Support Perturbation of
924 Lysosomal Function. Theranostics 7:2704-2717.
925 73. Edgar RC. 2013. UPARSE: highly accurate OTU sequences from microbial amplicon reads. Nat
926 Methods 10:996-8.
927 74. Quast C, Pruesse E, Yilmaz P, Gerken J, Schweer T, Yarza P, Peplies J, Glockner FO. 2013. The
928 SILVA ribosomal RNA gene database project: improved data processing and web-based tools.
929 Nucleic Acids Res 41:D590-6.
930 75. Eschenfeldt WH, Makowska-Grzyska M, Stols L, Donnelly MI, Jedrzejczak R, Joachimiak A. 2013.
931 New LIC vectors for production of proteins from genes containing rare codons. J Struct Funct
932 Genomics 14:135-44.
933 76. Gibson DG, Young L, Chuang RY, Venter JC, Hutchison CA, 3rd, Smith HO. 2009. Enzymatic
934 assembly of DNA molecules up to several hundred kilobases. Nat Methods 6:343-5.
935 77. Kwon K, Hasseman J, Latham S, Grose C, Do Y, Fleischmann RD, Pieper R, Peterson SN. 2011.
936 Recombinant expression and functional analysis of proteases from Streptococcus pneumoniae,
937 Bacillus anthracis, and Yersinia pestis. BMC Biochem 12:17.
938 78. Matulis D, Kranz JK, Salemme FR, Todd MJ. 2005. Thermodynamic stability of carbonic anhydrase:
939 measurements of binding affinity and stoichiometry using ThermoFluor. Biochemistry 44:5258-66.
940 79. Stephen J. Cavalieri IDR, Ronald J. Harbeck, Robert L. Sautter, Yvette S. McCarter, Susan E.
941 Sharp, José H. Ortez, Carol A. Spiegel. 2005. Manual of antimicrobial susceptibility testing.
942 American Society for Microbiology, Washington D.C.

943

944 ## Figure legends

945 **Fig. 1.** Variances in CB biomasses presented separately for each patient in box plots. We use the same
946 patient identifiers (P1 through P9) in the main text, other Figures, and Suppl. Datasets. P3 was not
947 included because only two data points were available. (m) male, (f) female. Biomass (abundance) pertains
948 to wet pellet weights in g x 10^{-2} for ~ 1.5-inch catheter pieces. The CB extracts were washed in PBS, thus
949 dissolving salt crystals that did not contribute to pellet weights. The horizontal bars depict statistically

950 significant weight differences comparing datasets from individual patients. Significance levels are coded
951 ***=0.001, **=0.01, and *=0.05, using the Wilcoxon rank sum test.

952 **Fig. 2.** Bacterial alpha-diversity using calculations based on the Shannon index. The Shannon index
953 accounts for abundance and evenness of OTUs. NE and SE: non-encrusted and salt-encrusted biofilms,
954 respectively. 16S rDNA data for UP and CB samples derived from the same timepoint were separate
955 entries**.** NE and SE diversities were statistically different based on a Wilcoxon rank sum test (P-value <
956 0.05)**.**

957 **Fig. 3.** Quantitatively represented microbial species according to metaproteomic data for CB and
958 associated UP samples. **A.** P1-P9, no evidence of salt crystals on catheter surfaces and in urine. **B.** P4-P7,
959 evidence of salt crystals on catheters and in urine. The bars are ordered from the first to last collection time
960 point (left to right). Collection time-matched CB and UP samples have the same number. The colored
961 segments of bars represent the abundances of microbial species, based on the sum of their PSMs relative
962 to the entire proteome identified from a sample. Horizontal bars at the top show the time frame of sample
963 collection. Vertical hatched bars separate UP from CB sample sets. Inserts display the times during which
964 antibiotics were administrated systemically (*BAC*, Bactrim; *CEF*, cefaroline-fosamil; *DAP*, daptomycin, *FLU*,
965 fluoconazole, *LEV*, levofloxacin).

966 **Fig. 4.** Variances in abundance for *P. mirabilis* (Pm) and *E. coli* (Ec) proteins. Proteins are listed with a
967 short name or gene locus. Locus and conserved sequence data predict the siderophore receptor role of
968 PMI2596. Statistical significance of protein variances is depicted by horizontal bars at the top of each box
969 plot. The significance levels are coded as ***=0.001, **=0.01, and *=0.05. The Wilcoxon rank sum test was
970 used to determine statistically significant differences in patient-to-patient comparisons (p-value < 0.05).

971 **Fig. 5.** Abundance correlations of proteins and molecular systems involved in TMI acquisition. The data
972 pertain to eight CB proteomes derived from P1. The bacterial species are Ef: *E. faecalis*; Pm: *P. mirabilis*;
973 and Ec: *E. coli*. Correlations were determined using the Pearson correlation method. Color intensity and
974 size of the circles are proportional to the correlation coefficients. Proteins are listed with UniProt short
975 names or gene loci.

Fig. 6. Studies on two predicted TMI-binding *E. faecalis* lipoproteins. **A.** EfaA abundance levels comparing CB data from five patients (see also legend, Fig. 4). Protein melting profiles (T_m) for **B.** EfaA and **C.** EF0577 binding SYPRO Orange for detection using the Light Cycler 480. Recombinant proteins (12.5 µM) were equilibrated in PBS containing 1 mM DTT. T_m profiles are shown for purified proteins (blue), proteins denatured with 6 M guanidine-HCl and washed with 8 M Urea to remove potential bound cofactors followed by renaturation with PBS (orange) or $CoCl_2$/PBS (grey) on a Ni-NTA agarose column. The concentrations of SYPRO Orange and $CoCl_2$, where applicable, were 8.3X and 50 µM, respectively.

Fig. 7. Neutrophil and eosinophil infiltration in response to persistent catheter colonization. **A.** Variation in MPO (PERM) and LTF (TRFL) abundance profiles for eight patients. Wilcoxon rank sum tests were used to assess variance. Statistically significant differences pertained to patient-to-patient comparisons (p-value < 0.05). **B.** Correlation analyses of neutrophil and eosinophil proteins were determined using the Pearson correlation method. Coloration is proportional to the correlation coefficients, and blank squares represent non-significant correlation (P-value < 0.05). Distinct clusters are boxed: this includes eosinophil peroxidase (PERE) and bone marrow proteoglycan PRG2; MPO and LTF clustered with cathepsin G (CATG), elastase (ELNE), and azurocidin (CAP7). **C.** MPO western blot data for samples derived from seven patients. Lane identifiers match UP sample identifiers also used in Fig. 3. Lane identifiers 40 (in P4 gel), 30 (in P5 gel) and 6 (in P6 gel) are not part of these patients' sample series. A The dominant 55 kDa band represents the processed MPO heavy chain (amino acid residues 279-745). Two patient 8 samples have a strong 20 kDa band, a fragment representing a C-terminal MPO fragment (the antibody is specific for a peptide sequence near the C-terminus). The protein loading is not normalized for uromodulin content. Therefore, staining intensities do not allow direct quantitative comparisons. M_r standards (St) in gels from top to bottom are: 100, 75, 50, 37, 25, and 20 kDa.

Table 1. Selected proteins representing different cell types and functions in innate immunity

UniProt ID	Rk[1] No.	A_{Avg} [2]	Protein name	Functional and cell surface biomarker roles for proteins [3]
P07911	1	3.05	Uromodulin (UMOD)	secreted from renal tubular cells into urine
P02788	2	2.02	Lactotransferrin (LTF)	abundant in activated neutrophils, iron-sequestering
P05164	4	1.55	Myeloperoxidase (MPO)	abundant in activated neutrophils (azurophilic granules)
P13646	5	1.50	Keratin, type I cytoskeletal 13 (KRT13)	abundant in stratified squamous epithelial cells
P01024	7	1.32	Complement system component C3	abundant effector of the complement system
P06702	10	0.89	Protein S100-A9 (calgranulin)	abundant in activated neutrophils, Zn^{2+} sequestering

P05109	32	0.45	Protein S100-A8 (calgranulin)	abundant in activated neutrophils, Zn^{2+} sequestering
P68871	46	0.33	Hemoglobin subunit beta (HBB)	abundant in erythrocytes
P11678	51	0.28	Eosinophil peroxidase (EPX)	abundant in activated eosinophils (secreted granules)
P80188	92	0.14	Lipocalin-2 (LCN2)	abundant in activated neutrophils (gelatinase granules)
P31997	252	0.04	Carcinoembryonic antigen-related cell adhesion molecule 8 (CEACAM8)	granulocyte cell-specific surface marker [3]
Q8N6Q3	421	0.02	CD177 antigen (CD177)	neutrophil cell-specific granule and surface marker [3]
P20702	769	0.01	Integrin alpha-X (ITGAX)	T-cell, B-cell, NK-cell, DC, MAC/monocyte, granulocyte cell-specific marker [3.4]
P16422	940	<0.01	Epithelial cell adhesion molecule (EPCAM)	epithelial cell specific marker [3]
O00526	2484	<0.01	Uroplakin-2	urothelial umbrella cell-specific marker (bladder)
P09693	4898	<0.01	T-cell surface glycoprotein CD3 γ chain	T-cell-specific surface marker [3]
P20138	8191	<0.01	Myeloid cell surface antigen CD33	DC, granulocyte, MAC/monocyte, stem cell marker [3.4]
P15391	8238	<0.01	B-lymphocyte antigen CD19	B cell, DC and stem cell surface marker [3.4]

[1]Normalized abundance rank and [2]Normalized relative protein quantity average from all UP and CB datasets (the PSMs matched to a protein divided by the sum of all human PSMs); [3]Cell differentiation marker according to (33); [4]abbr.: DC, dendritic cells; MAC: macrophages; NK, natural killer cells;

Table 2. Antimicrobial drug resistance of bacterial strains isolated from P1, P2, P7 and P9

Bacterial species	**Sample source**	**Ampicillin** 100 µg	**Cefotaxime** 30 µg	**Cephalexin** 30 µg	**Ciprofloxacin** 5 µg	**Sulfanilamide / TMT** 200µg/ 12µg	**Gentamycin** 30 µg
P. aeruginosa (P1)	19CB	0.6	NP	NP	2.7	0.6	NP
K. pneumoniae (P2)	43CB	0.6	0.6	NP	0.6	NP	1.4
P. mirabilis (P7)	65CB	2.2	NP	2.4	2.1	2.0	1.0
S. marcescens (P9)	74UP	2.2	NP	NP	2.2	1.9	NP
E. faecalis (P9)	74UP	2.0	NP	0.6	0.6	0.6	NP
S. aureus (P9)	75UP	1.1	NP	0.8	0.6	3.2	1.6

All disk diffusion tests were performed in three replicates using Mueller-Hinton agar. The *E. faecalis* isolate was also grown on blood agar yielding the same results. The data provided here are growth clearance zones in cm (disk diameter 0.6 cm). Abbr: P: patient; NP: susceptibility tests were not performed. TMT: trimethoprim.

Table 3. Sequences of PCR primers

Gene Name	Signal peptide	Primers	
EF_3082	1-31	Forward	5'-CGAGAACCTGTACTTCCAATCCAATGCAACAACAGAAACAACAGCTA
		Reverse	5'-TTCGGATCCGTTATCCACTTCCAATTTACTCTAATCCTTTTTTAACATCTTC
EF_0577	1-26	Forward	5'-CGAGAACCTGTACTTCCAATCCAATACAAATAGTAAAGACAAAGATACAGT
		Reverse	5'-TTCGGATCCGTTATCCACTTCCAATTTATTTCGAAAGGCCTTCAGCA
EF_2076	1-24	Forward	5'-CGAGAACCTGTACTTCCAATCCAATGCTGAAAAGAAAGAAAAATTAGCAATT
		Reverse	5'-TTCGGATCCGTTATCCACTTCCAATTTATTTACTCATTAAGCCATCATGG

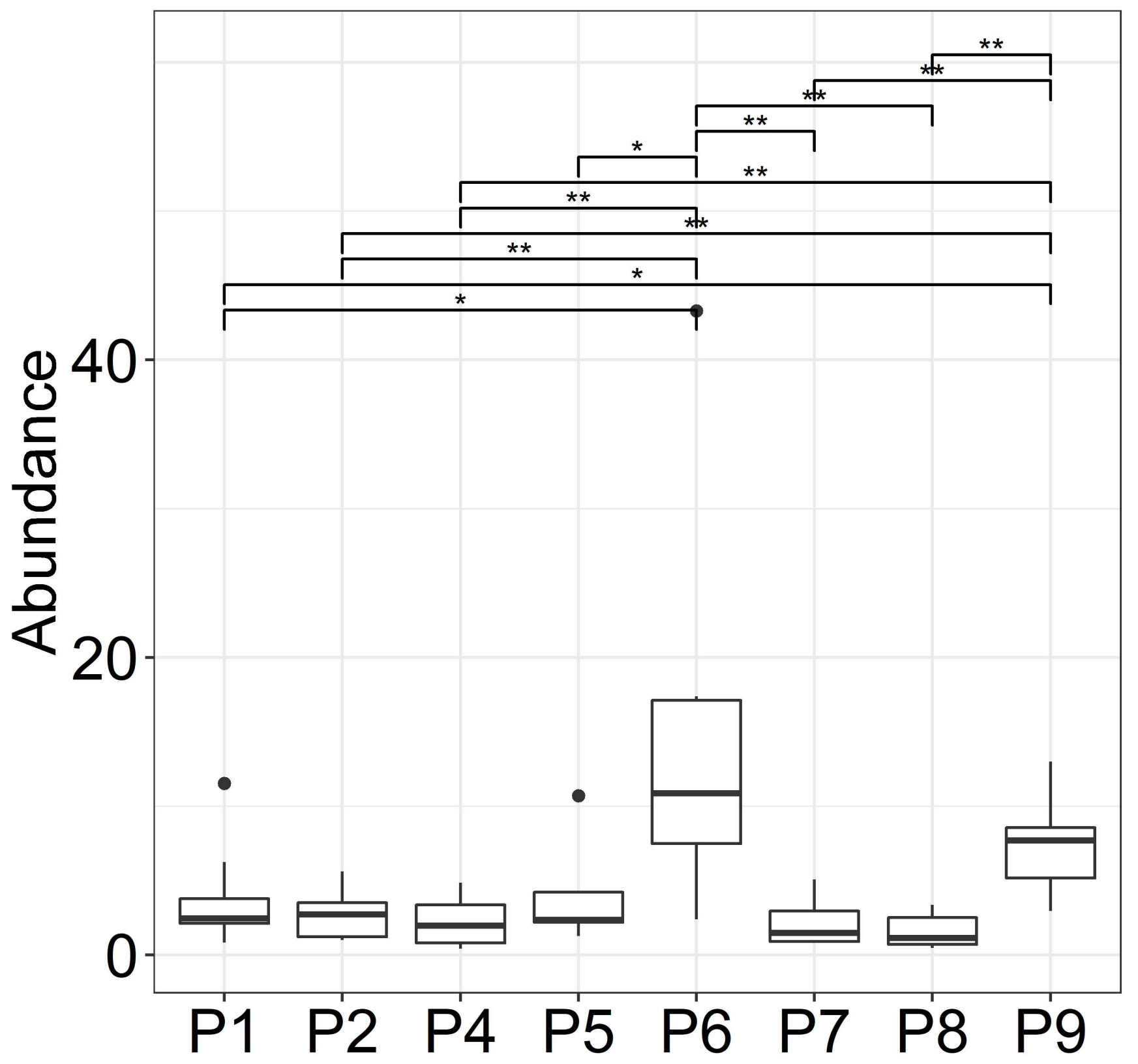
Abundance
40
20
0
P1
P2
P4
P5
P6
P7
P8
P9
*
*
**
**
**
**
**
**
**
**
**

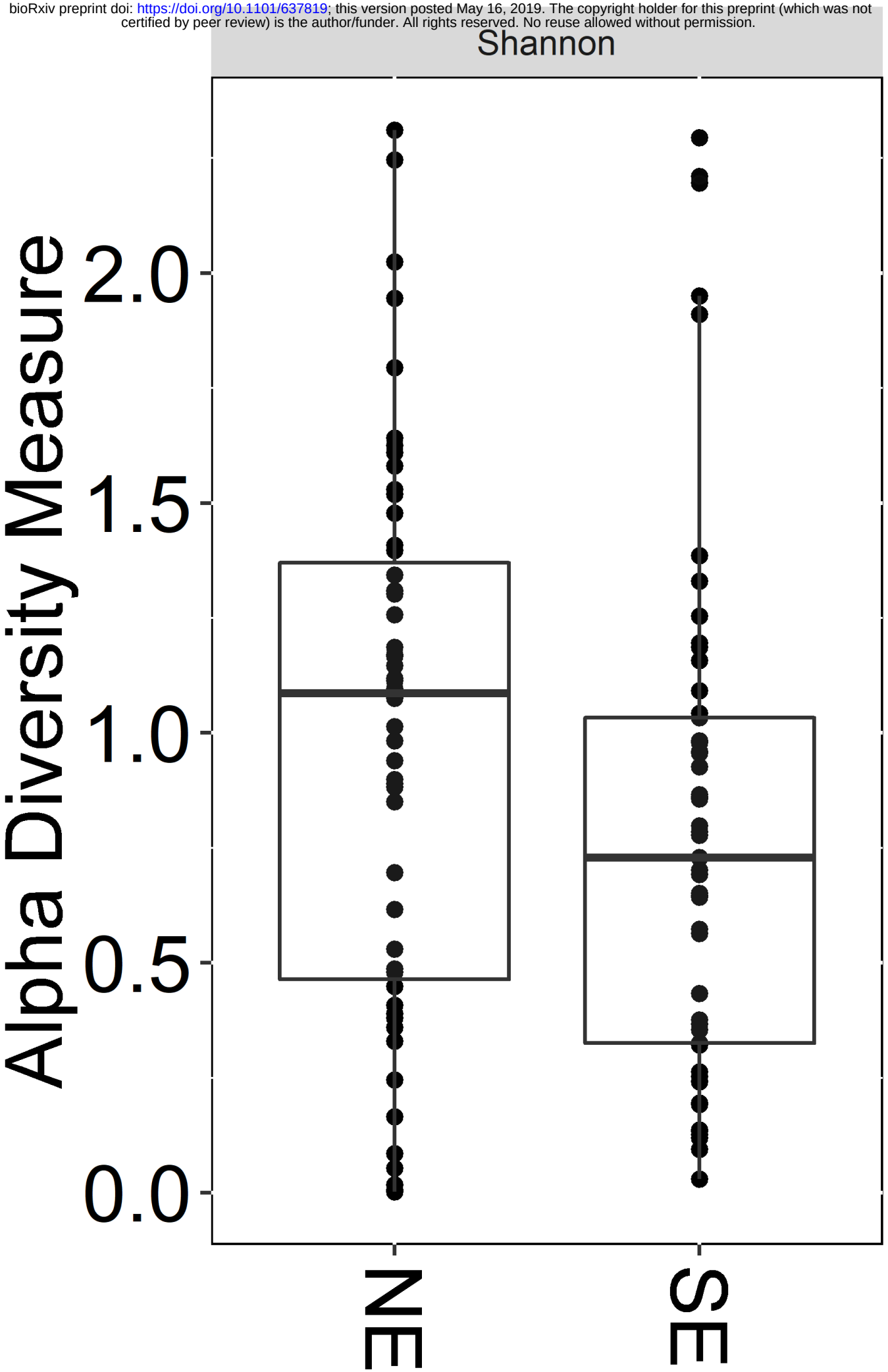

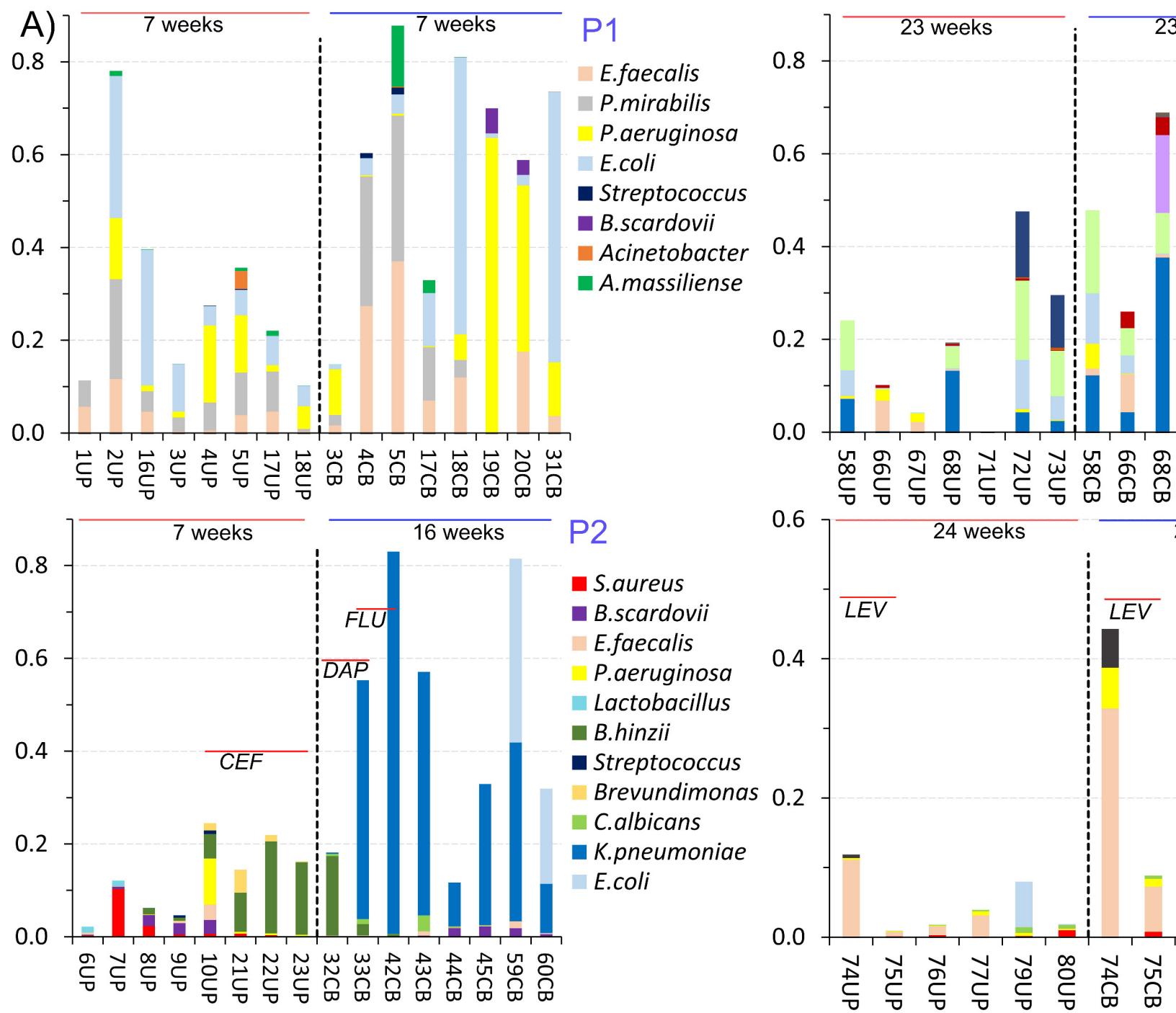
A)
7 weeks
7 weeks
P1
E.faecalis
P.mirabilis
P.aeruginosa
E.coli
Streptococcus
B.scardovii
Acinetobacter
A.massiliense
0.0
0.2
0.4
0.6
0.8
1UP
2UP
16UP
3UP
4UP
5UP
17UP
18UP
3CB
4CB
5CB
17CB
18CB
19CB
20CB
31CB
23 weeks
23
58UP
66UP
67UP
68UP
71UP
72UP
73UP
58CB
66CB
68CB
7 weeks
16 weeks
P2
S.aureus
B.scardovii
E.faecalis
P.aeruginosa
Lactobacillus
B.hinzii
Streptococcus
Brevundimonas
C.albicans
K.pneumoniae
E.coli
CEF
FLU
DAP
6UP
7UP
8UP
9UP
10UP
21UP
22UP
23UP
32CB
33CB
42CB
43CB
44CB
45CB
59CB
60CB
24 weeks
LEV
LEV
74UP
75UP
76UP
77UP
79UP
80UP
74CB
75CB

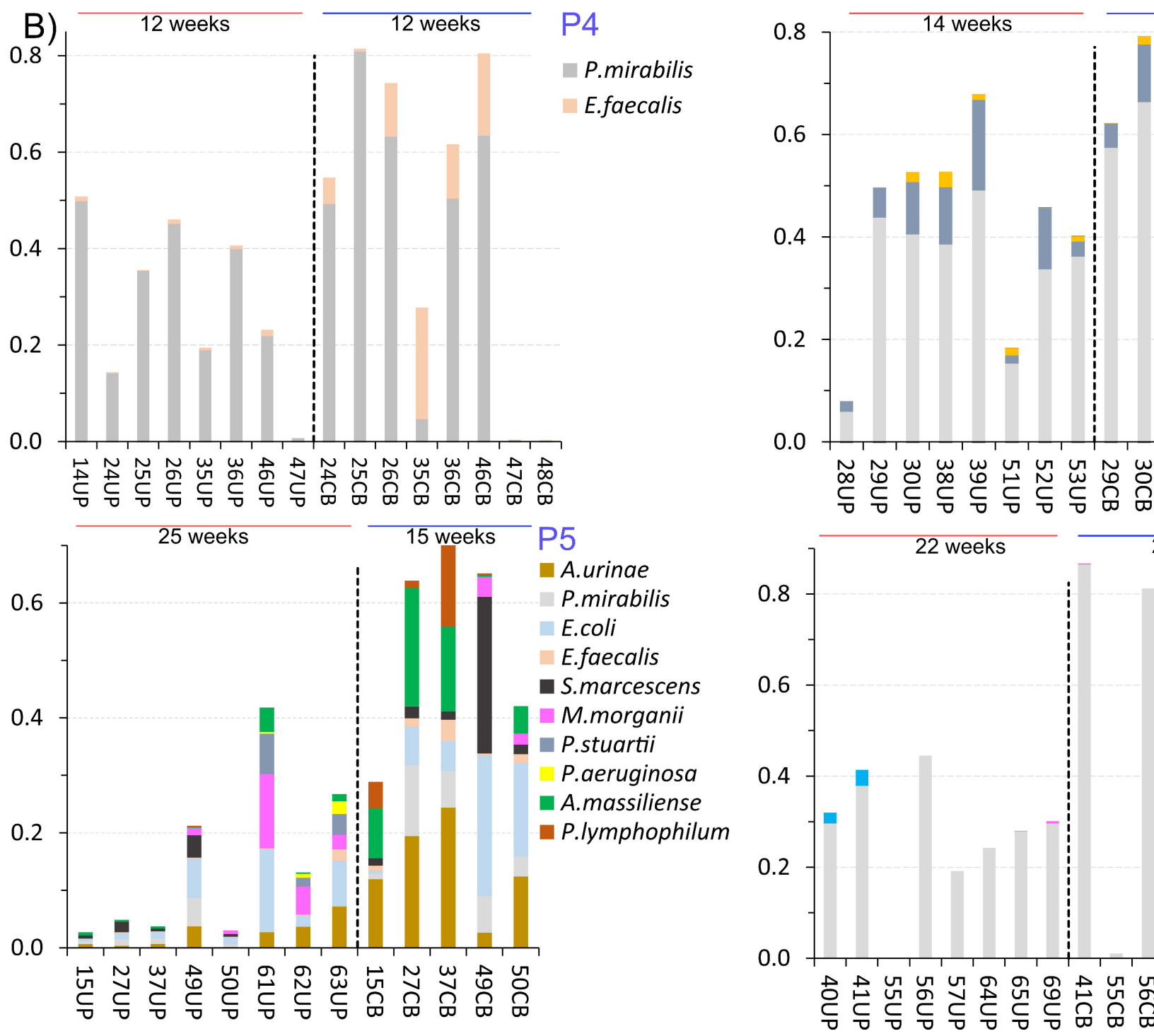
B)
12 weeks
12 weeks
P4
P.mirabilis
E.faecalis
0.0
0.2
0.4
0.6
0.8
14UP
24UP
25UP
26UP
35UP
36UP
46UP
47UP
24CB
25CB
26CB
35CB
36CB
46CB
47CB
48CB
14 weeks
28UP
29UP
30UP
38UP
39UP
51UP
52UP
53UP
29CB
30CB
25 weeks
15 weeks
P5
A.urinae
P.mirabilis
E.coli
E.faecalis
S.marcescens
M.morganii
P.stuartii
P.aeruginosa
A.massiliense
P.lymphophilum
15UP
27UP
37UP
49UP
50UP
61UP
62UP
63UP
15CB
27CB
37CB
49CB
50CB
22 weeks
40UP
41UP
55UP
56UP
57UP
64UP
65UP
69UP
41CB
55CB
56CB

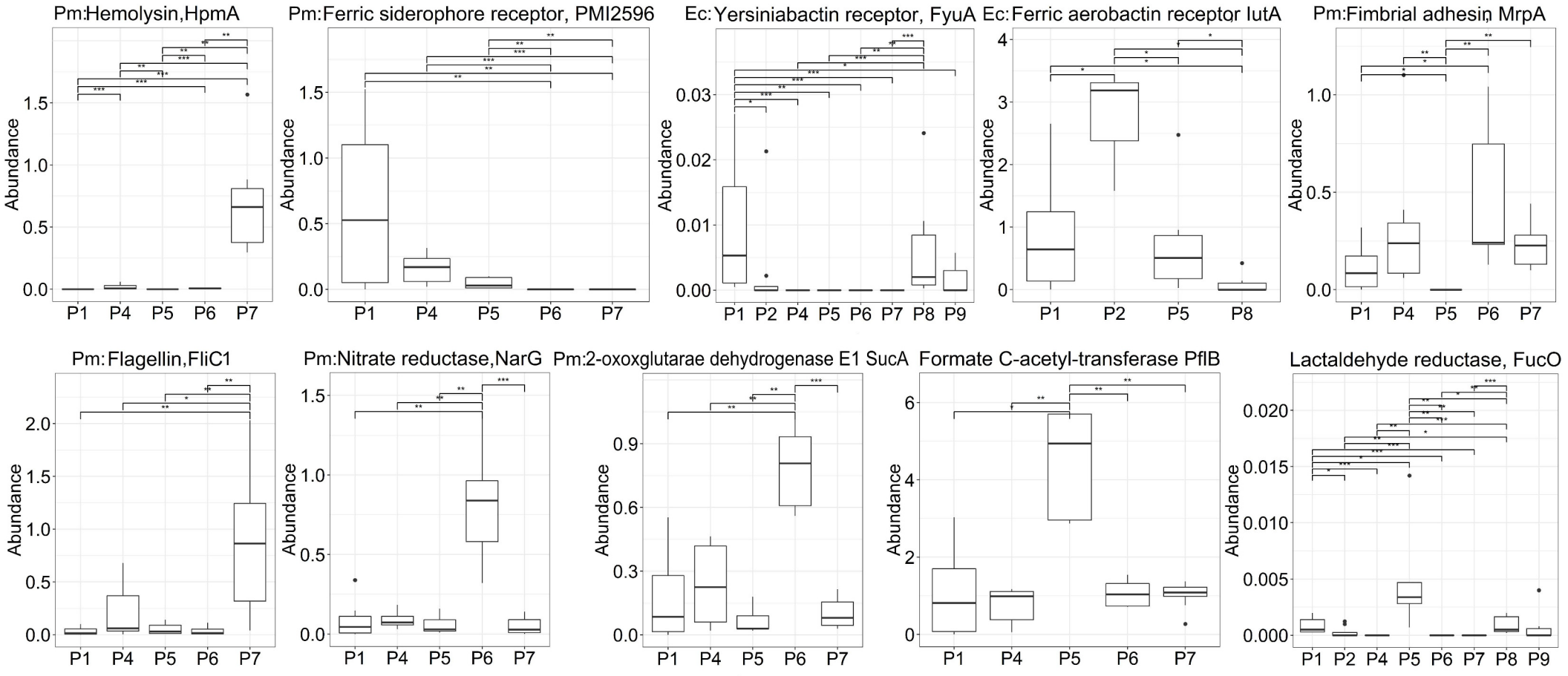
Pm:Hemolysin,HpmA
Pm:Ferric siderophore receptor, PMI2596
Ec:Yersiniabactin receptor, FyuA
Ec:Ferric aerobactin receptor IutA
Pm:Fimbrial adhesin MrpA
Pm:Flagellin,FliC1
Pm:Nitrate reductase,NarG
Pm:2-oxoxglutarae dehydrogenase E1 SucA
Formate C-acetyl-transferase PflB
Lactaldehyde reductase, FucO
Abundance
P1 P4 P5 P6 P7
P1 P2 P4 P5 P6 P7 P8 P9
P1 P2 P5 P8
P1 P4 P5 P6 P7

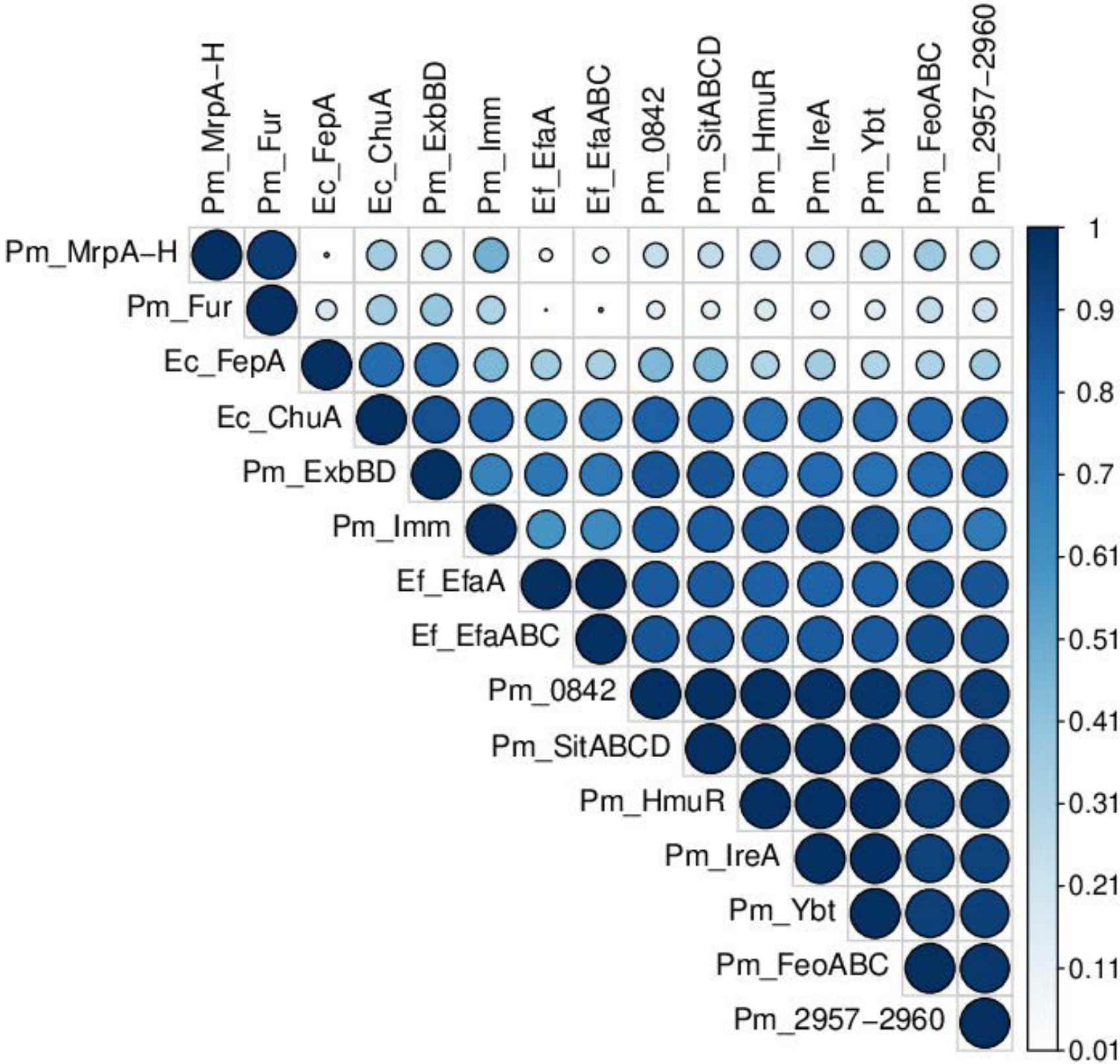
Pm_MrpA−H
Pm_Fur
Ec_FepA
Ec_ChuA
Pm_ExbBD
Pm_Imm
Ef_EfaA
Ef_EfaABC
Pm_0842
Pm_SitABCD
Pm_HmuR
Pm_IreA
Pm_Ybt
Pm_FeoABC
Pm_2957−2960
1
0.9
0.8
0.7
0.61
0.51
0.41
0.31
0.21
0.11
0.01

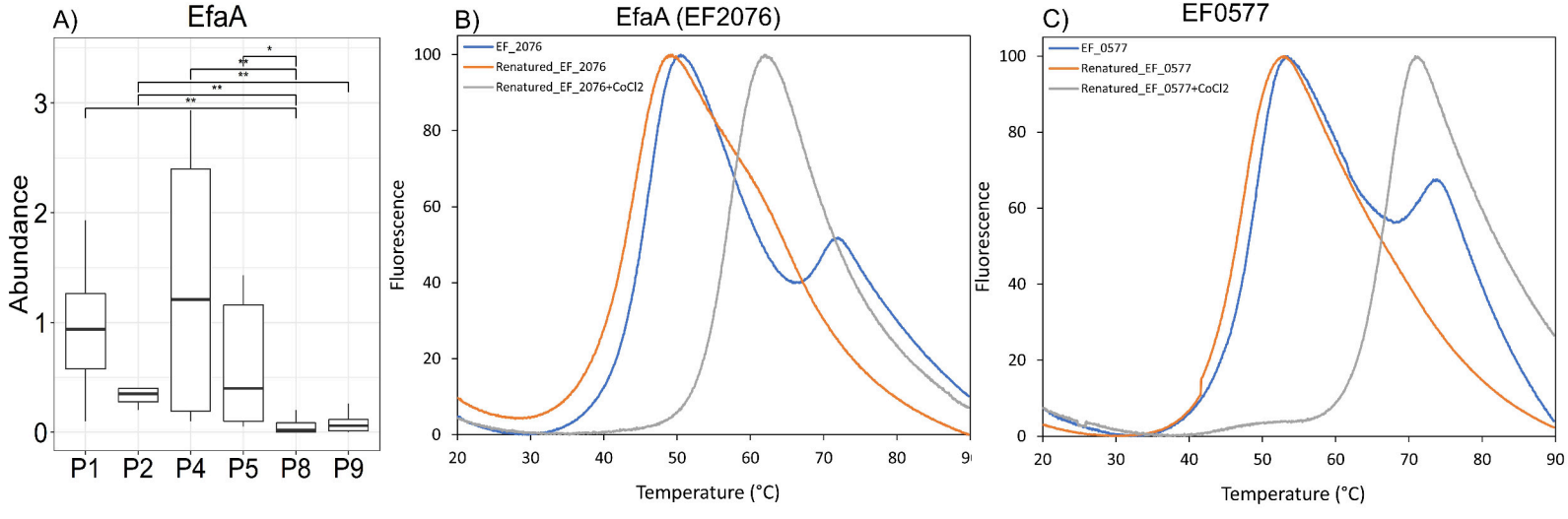
A)
EfaA
Abundance
P1
P2
P4
P5
P8
P9
B)
EfaA (EF2076)
EF_2076
Renatured_EF_2076
Renatured_EF_2076+CoCl2
Fluorescence
Temperature (°C)
C)
EF0577
EF_0577
Renatured_EF_0577
Renatured_EF_0577+CoCl2
Fluorescence
Temperature (°C)

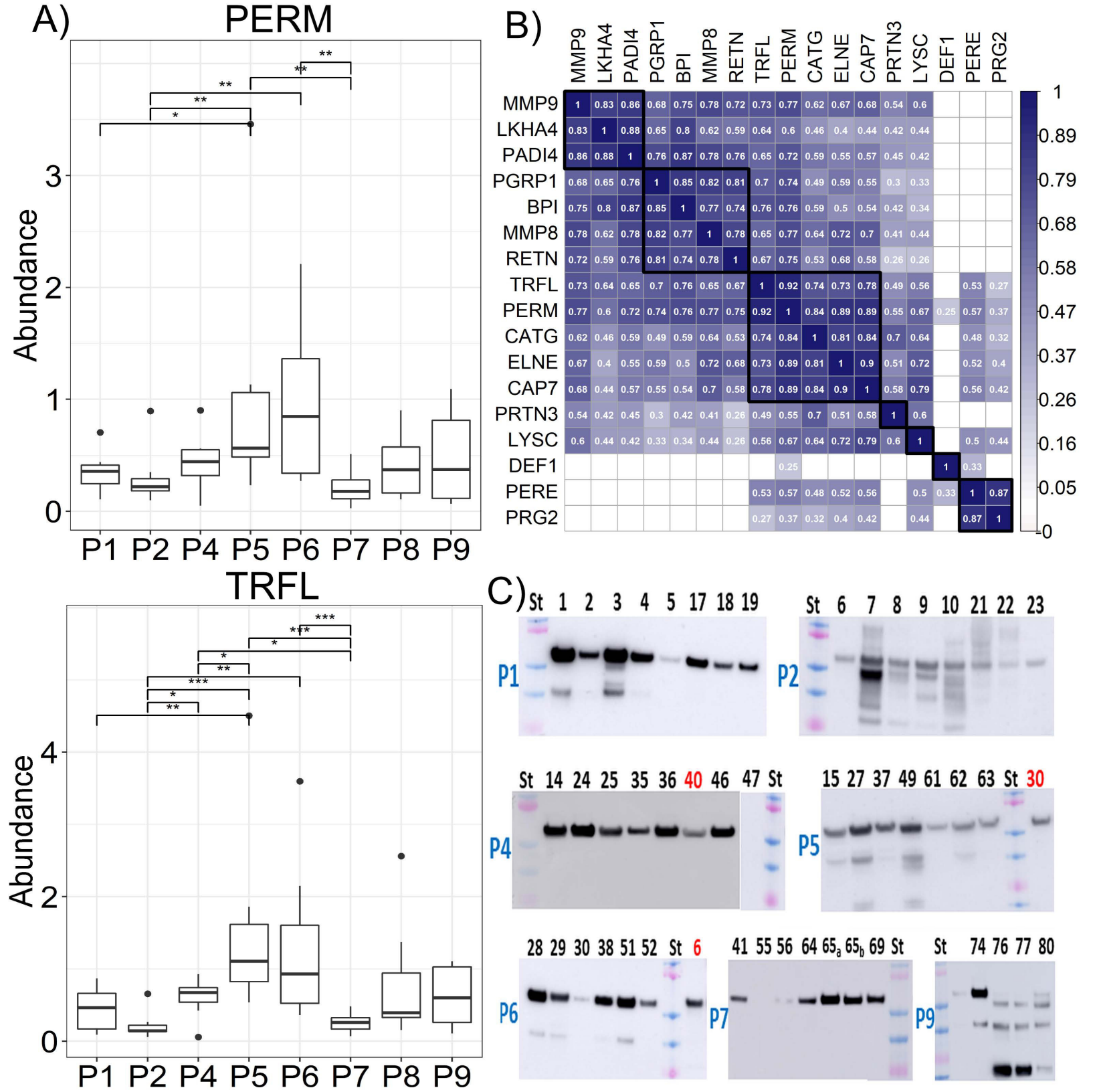
A)
PERM
Abundance
P1 P2 P4 P5 P6 P7 P8 P9
TRFL
Abundance
P1 P2 P4 P5 P6 P7 P8 P9
B)
MMP9 LKHA4 PADI4 PGRP1 BPI MMP8 RETN TRFL PERM CATG ELNE CAP7 PRTN3 LYSC DEF1 PERE PRG2
MMP9 1 0.83 0.86 0.68 0.75 0.78 0.72 0.73 0.77 0.62 0.67 0.68 0.54 0.6
LKHA4 0.83 1 0.88 0.65 0.8 0.62 0.59 0.64 0.6 0.46 0.4 0.44 0.42 0.44
PADI4 0.86 0.88 1 0.76 0.87 0.78 0.76 0.65 0.72 0.59 0.55 0.57 0.45 0.42
PGRP1 0.68 0.65 0.76 1 0.85 0.82 0.81 0.7 0.74 0.49 0.59 0.55 0.3 0.33
BPI 0.75 0.8 0.87 0.85 1 0.77 0.74 0.76 0.76 0.59 0.5 0.54 0.42 0.34
MMP8 0.78 0.62 0.78 0.82 0.77 1 0.78 0.65 0.77 0.64 0.72 0.7 0.41 0.44
RETN 0.72 0.59 0.76 0.81 0.74 0.78 1 0.67 0.75 0.53 0.68 0.58 0.26 0.26
TRFL 0.73 0.64 0.65 0.7 0.76 0.65 0.67 1 0.92 0.74 0.73 0.78 0.49 0.56 0.53 0.27
PERM 0.77 0.6 0.72 0.74 0.76 0.77 0.75 0.92 1 0.84 0.89 0.89 0.55 0.67 0.25 0.57 0.37
CATG 0.62 0.46 0.59 0.49 0.59 0.64 0.53 0.74 0.84 1 0.81 0.84 0.7 0.64 0.48 0.32
ELNE 0.67 0.4 0.55 0.59 0.5 0.72 0.68 0.73 0.89 0.81 1 0.9 0.51 0.72 0.52 0.4
CAP7 0.68 0.44 0.57 0.55 0.54 0.7 0.58 0.78 0.89 0.84 0.9 1 0.58 0.79 0.56 0.42
PRTN3 0.54 0.42 0.45 0.3 0.42 0.41 0.26 0.49 0.55 0.7 0.51 0.58 1 0.6
LYSC 0.6 0.44 0.42 0.33 0.34 0.44 0.26 0.56 0.67 0.64 0.72 0.79 0.6 1 0.5 0.44
DEF1 0.25 1 0.33
PERE 0.53 0.57 0.48 0.52 0.56 0.5 0.33 1 0.87
PRG2 0.27 0.37 0.32 0.4 0.42 0.44 0.87 1
1 0.89 0.79 0.68 0.58 0.47 0.37 0.26 0.16 0.05 0
C)
St 1 2 3 4 5 17 18 19
P1
St 6 7 8 9 10 21 22 23
P2
St 14 24 25 35 36 40 46 47 St
P4
15 27 37 49 61 62 63 St 30
P5
28 29 30 38 51 52 St 6
P6
41 55 56 64 65a 65b 69 St
P7
St 74 76 77 80
P9